CCM-80-16

Center for Composite Materials

FAILURE ANALYSES OF COMPOSITE BOLTED JOINTS

NASA Grant 1409

D. W. Wilson
J. W. Gillespie
J. L. York
R. B. Pipes

College of Engineering
University of Delaware
Newark, Delaware

FAILURE ANALYSES OF COMPOSITE BOLTED JOINTS

D. W. Wilson
J. W. Gillespie
J. L. York
R. B. Pipes

Center for Composite Materials
University of Delaware
Newark, Delaware 19711

Sponsored by

NASA Grant 1409
NASA Langley Research Center
Hampton, Virginia 23665

July 1980

Failure Analyses of Composite Bolted Joints

ABSTRACT

The complex failure behavior exhibited by composite bolted joints of graphite-epoxy (Hercules AS/3501) has been investigated for the net tension, bearing and shearout failure modes using combined analytical and experimental techniques. Plane stress, linear-elastic, finite-element methods were employed to determine the two-dimensional state of stress resulting from a loaded hole in a finite-width, semi-infinite strip. The stresses predicted by the finite-element method were verified by experiment to lend credence to the analysis. Both numerical and experimental parametric studies were conducted to investigate the influence of joint geometric parameters on the state of stress and resultant strength of the joint. The resulting functional relationships found to exist between bolted joint strength and the geometric parameters, bolt diameter (D), e/D and W/D, were applied in the formulation of semi-empirical strength models for the basic failure modes. A point stress failure criterion was successfully applied as the failure criterion for the net tension and shearout failure modes. The bearing failure mode could not be accurately modeled using

two-dimensional plane-stress, finite-element analysis in combination with any known failure criterion although a maximum bearing stress criterion serves as a good order of magnitude estimate. Thus, using the results of the parametric studies, experimental test data and the point stress failure criterion, shearout and net tension strength models have been developed which account for the effects of geometry in composite bolted joint strengths. The implications of the results from this study on the further development of comprehensive bolted joint failure models for use in the efficient design composite bolted joints is discussed.

TABLE OF CONTENTS

NOMENCLATURE

Term	Description
edge distance (e)	Distance from center of hole to the end edge of the laminate.
hole diameter (D)	The diameter of the fastener hole.
width (W)	Width of the coupon which is equivalent to the half spacing between fasteners.
pin loading	Reacting the joint loads with a pin which offers no out-of-plane restraint.
out-of-plane constraint	Reacting the joint loads through the pin while constraining the out-of-plane deformations (deformations normal to plane of laminate).
bearing failure	A failure where localized crushing of the material reacting load leads to an elongation of the hole.
shear-out failure	Failure which is characterized by extensive cleavage damage parallel to the loading extending from the two sides of the fastener hole to the edge of the coupon.
net tension failure	Normal tensile failure occurring in the material adjacent to the fastener hole.
ultrasonic "C" scan	A nondestructive inspection technique which uses ultrasonic waves to reveal information about the structure of the material.
point stress failure criterion	A failure criterion which predicts failure when the stress adjacent to a notch at a critical distance d_o reaches the unnotched laminate strength.

LIST OF FIGURES

LIST OF TABLES

INTRODUCTION

Advanced composites are being considered for many load bearing structural applications requiring mechanically fastened joints. The cutouts required for mechanical fasteners always result in reduced structural load carrying efficiency and in composites this problem is amplified by the anisotropic nature of the material. The material anisotropy and brittleness intensify the stress concentration effects and provides for competing failure modes, each of which may be catastrophic. As a result the failure strength and mode of composite bolted joints are strongly dependent upon the material properties, laminate configuration and joint geometry. The development of a comprehensive composite bolted joint analysis procedure hinges upon understanding the influence of these parameters upon bolted joint strength and failure mode.

The development of a comprehensive composite bolted joint analysis procedure involves the analytic determination of the state of stress/strain in the joint element and application of an appropriate failure criterion. The closed-form solution to the elasticity problem of a loaded hole with a rigid inclusion in a finite-width, semi-infinite, anisotropic plate is intractable, hence numerical methods

must be used to determine the state of stress in the joint. Both finite-element [1-4] and approximate elasticity solutions [5,6] have been developed for the plane stress analysis of the stresses in an anisotropic plate loaded by a frictionless pin. The choice of an appropriate failure criterion has been the deficiency of most analyses. Distortional energy [1,2], Tsai-Wu [3], Maximum stress, Fracture Toughness [7], and Average Stress failure criteria [8] have all been employed with various degrees of success. An acceptable degree of accuracy and reliability has not been obtained with any one of the above criteria for all failure modes primarily because there are different failure mechanisms associated with each mode and no single criterion can model them all. The task remains, therefore, to identify the appropriate failure criterion for each failure mode.

Empirical data are required for the verification of any analytical model or failure criterion. A substantial data base has been developed characterizing the effects of joint geometry [9], laminate configuration [9-13], stacking sequence [14], elevated temperature [15,16] and moisture concentration [17,18] on composite bolted joint performance. Results from these experimental investigations provided valuable insight into the failure behavior of composite bolted joints which the authors used in the formulation of analytical failure models herein.

In this study parallel experimental and analytical characterization of bolted joint behavior was conducted in an attempt to develop semi-empirical strength models for each of the three primary failure modes: net tension, shearout, and bearing. A two-dimensional, plane-stress, orthotropic, finite-element analysis was used to determine the state of stress around the loaded hole in a finite-width, semi-infinite orthotropic strip. The stress information obtained by the finite element analysis was then combined with the failure criteria to predict strengths. Observed similarities between the failure behavior of notched composites and mechanically fastened composite joints suggested that the point stress failure criterion might be successfully applied to the shearout and not tension failure modes. The bearing failure mode has been shown to be dependent on the multiaxial state of stress and thus the Tsai-Wu criterion was considered.

It is important to point out that the failure criteria proposed in the development of the bolted joint strength models are based on intrinsic material properties which are experimentally determined using appropriate test methods. This leads to the desirable result that the design of bolted joints can be accomplished using specific material properties instead of empirical bolted joint strength data. Thus the development of a reliable, comprehensive bolted joint strength analysis could lead

to substantial reductions in the size of the empirical data base required for bolted joint design.

EXPERIMENTAL PROCEDURE

Data characterizing the effect of joint geometry (i.e. e/D and w/D) on strength and failure mode has been generated previously [15]. The experimental program conducted in this study was designed to determine the basic material properties (E_x, E_y, ν_{xy}, G_{xy}, S_x^T, S_x^C, S_y^T and S_{xy}) of the designated AS/3501-6 graphite/epoxy laminate and to determine the notched strength behavior for a range of circular notch sizes loaded under bolted joint conditions. A set of specimens was designed to exhibit each of the three primary failure modes holding e/D and w/D constant, while varying bolt diameter, D. Several specimens were instrumented for verification of the finite element analysis. The details of this experimental program are discussed below.

Specimen Fabrication

The test specimens for both the material characterization study and the fastener size effect study were fabricated from a single lot of Hercules AS/3501-6 graphite/epoxy prepreg. The laminate configuration was $[45/0/-45/0_2/-45/0/45/0_2/90]_s$ which resulted in a cured panel thickness of 3.0 mm (0.118 in.) using manufacturer recommended autoclave processing

procedures. All laminates were ultrasonically inspected for processing related flaws to insure the exclusion of the flawed material from the test program.

The test specimens used for the material characterization study were of standard configurations for tensile tests, IITRI compression tests and two-rail, shear tests. Details of the test procedure, fixturing and specimen geometry can be found in the literature [19,20,21]. The bolted joint specimen was of the same single fastener design described by Wilson and Pipes in an earlier report [15] and is shown in Figure 1.

Test coupons were machined to size using a diamond saw to minimize machining-induced damaged. Similarly, diamond core drills were used to machine the 3.2 mm (0.125 in.), 6.4 mm (0.250 in.) and 9.5 mm (0.375 in.) holes in the specimens. The integrity of the machined specimens was verified using ultrasonic inspection and any flawed coupons were discarded from the test program. Width, thickness, hole diameter and hole location dimensions were recorded for each specimen.

Testing Procedure

The general test procedures used in the material characterization tests are well documented and will not be reiterated in this report. However, specific procedural

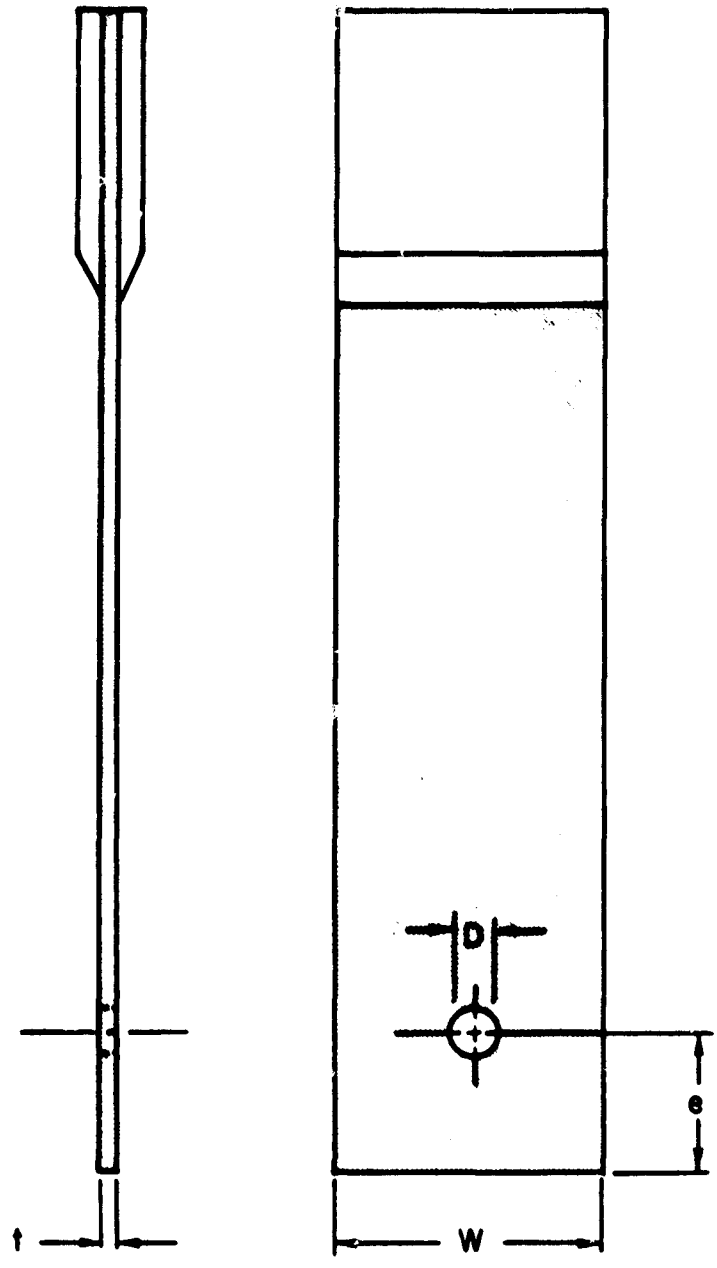

Figure 1. Bolted Joint Test Specimen Geometry

aspects of the test program are reported herein for completeness.

The specimens were loaded by a floor model TTC Instron test machine at a crosshead speed of 0.02 cm/min. Strengths were determined by observing the maximum load carried by the specimen as determined by the load-deflection curve. Deformations were measured using electrical-resistance foil strain gages and digital strain instrumentation. Modulus measurement utilized gages with a 6.35 mm (0.1250 in.) grid and point strain measurements used gages with a 0.38 mm (0.015 in.) grid length. Strain measurements were typically taken at 98 Nt load increments. A minimum of three specimens were tested to determine each material property and three replicates of each bolted joint configuration were tested.

The testing procedure used for the bolted joint tests was similar to that used for the standard static tensile property characterization. A specially designed clevis fixture (Fig. 2) was used to simulate bolted load reaction through the hole in the coupon while standard wedge action friction grips introduced load at the tabbed end of the specimen. For the pinned tests the load was reacted by a high strength steel pin and no constraining contact was allowed on the laminate surface surrounding the pin. To simulate out of plane constraint annular

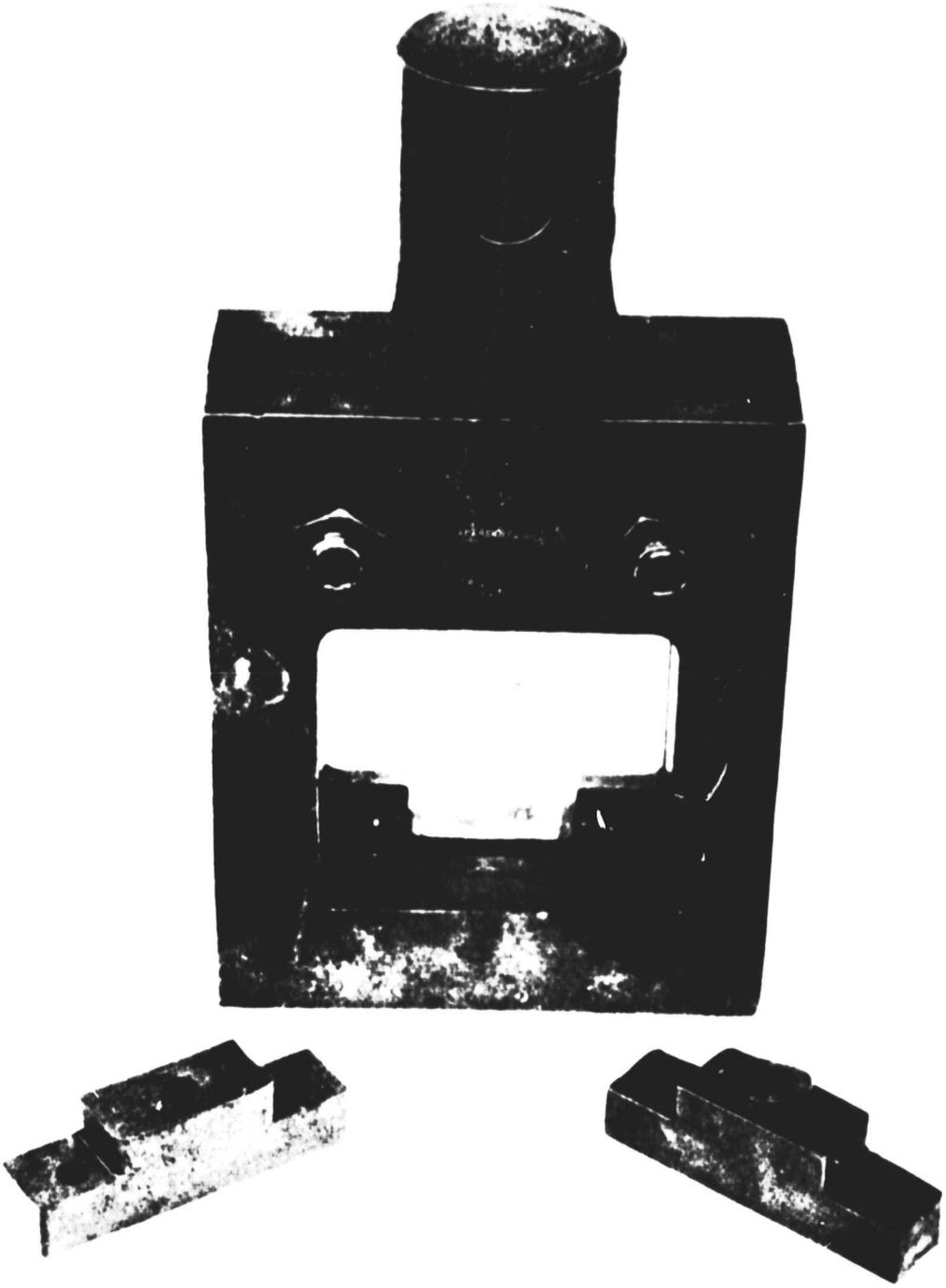

Figure 2. Bolted Joint Test Fixture

washers with an inside diameter equal to the pin diameter and an outside diameter equal to twice the pin diameter were employed. Various sizes of pins and washers were available to insure excellent fit of the washer to the pin and the pin to the fastener hole. The torques applied to the simulated fasteners were defined as finger tight. The effect of fastener fit and torque on bolted joint strength is significant and is discussed in later sections.

Failure Strength Analysis

The ability of analytical models to describe composite bolted joint strength and failure mode behavior is dependent upon the knowledge of the state of stress and application of appropriate failure criteria. A finite-element model was developed to analyze the state of stress for the bolted joint geometries and loadings considered in this program. Stress profiles predicted by the finite-element model along the critical failure planes defined in Figure 3 for the bearing, shearout and net tension modes were determined and verified by experiment. Functional representations of these stress profiles including the parametric effects of geometry were then developed for combination with the failure criteria. Based on simularities observed between notched strength and bolted joint failure behavior the effectiveness of the

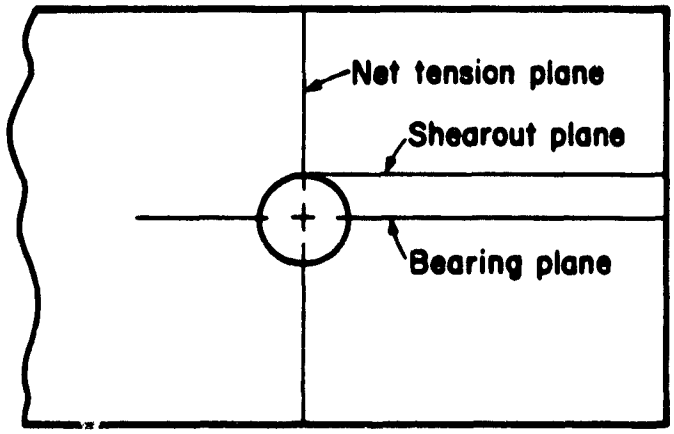

Figure 3. Description of the Failure Planes for the Three Failure Modes

"point stress" criterion was investigated for the net tension and shearout failure modes. The Tsai-Wu failure criterion was studied for the bearing failure mode because of the known effects of the multiaxial state of stress in the bearing failure zone. Semi-empirically based, closed-form relationships result from the introduction of the approximate stress functions into the failure criteria which can be used to predict composite bolted joint strengths.

The Structural Analysis Program SAPV was used to develop a two-dimensional linear-elastic finite element model of a composite bolted joint. The model employed the plane-stress, quadrilateral element with orthotropic material properties to form the mesh subjected to the boundary conditions depicted in Figure 4. The bolted joint was treated as a loaded hole containing a frictionless rigid inclusion in a finite-width semi-infinite strip. Sixteen different geometric variations of the model were developed to analyze the effects of geometric parameters e/D and w/D on the state of stress. The experimentally determined material properties used in the finite element model and in the failure criteria are listed in Table 1.

The stress profiles developed along the three critical failure planes are plotted in non-dimensional form in Figures 5-7. Only the primary stress component important

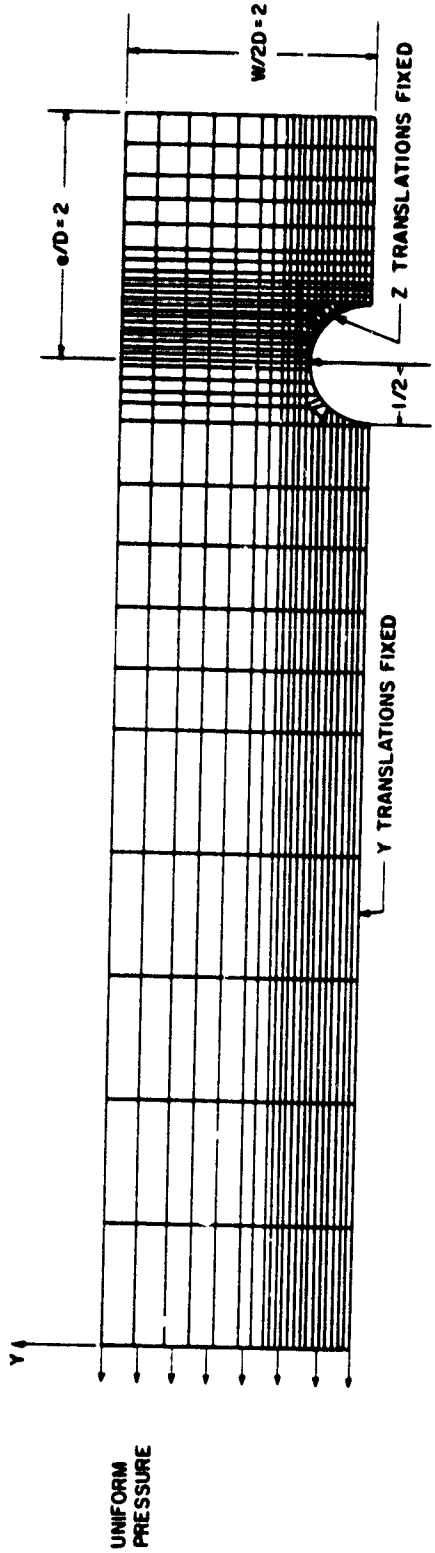

Figure 4. Finite Element Model Used to Analyze the Bolted Joint

Table 1.

Material and Strength Properties

Property	Value		
E_x	$10.9\ 10^6$ psi	75.2	GPa
E_y	$4.39\ 10^6$ psi	30.3	GPa
ν_{xy}	0.397		
ν_{yx}	0.160		
G_{xy}	$2.00\ 10^6$ psi	13.8	GPa
$\sigma^{ult}_{x,tens}$	131.0 ksi	903.2	MPa
$\sigma^{ult}_{y,tens}$	45.2 ksi	311.6	MPa
$\sigma^{ult}_{x,comp}$	140.0 ksi	965.0	MPa
τ^{ult}_{xy}	21.7 ksi	149.6	MPa

to each failure mode is presented (i.e. shear stress for shearout, tensile stress for net tension, etc.). To develop confidence in the stresses predicted by the finite-element model along the critical planes for the net tension, shearout and bearing failure modes, specimens were instrumented with strain gages along these planes. The gage grid layers were 0.381 mm (0.015 in.) and thus closely approximated point strain measurements for comparison with the finite-element predicted values. The data plotted in Figures 5-7 summarize the results for the net tension, shearout and bearing modes respectively. The strain results showed relatively poor agreement with the finite-element predicted strains along the net tension plane (Fig. 5) but a plot of the strains along a plane 0.25 mm (0.01 in.) above the net section plane showed excellent agreement with the experimental results. Normal strain component measurements taken at 45° to the shearout plane agree well with the finite-element predictions as shown in Fig. 6. The bearing strains predicted by finite elements exhibited the proper trend but did not agree closely with the measured values (Fig. 7). The relatively close agreement away from the hole tends to indicate that the stresses are much greater near the hole than predicted by the model. This result could be due to some outer ply buckling behavior or inaccurate modeling of the bolt-joint

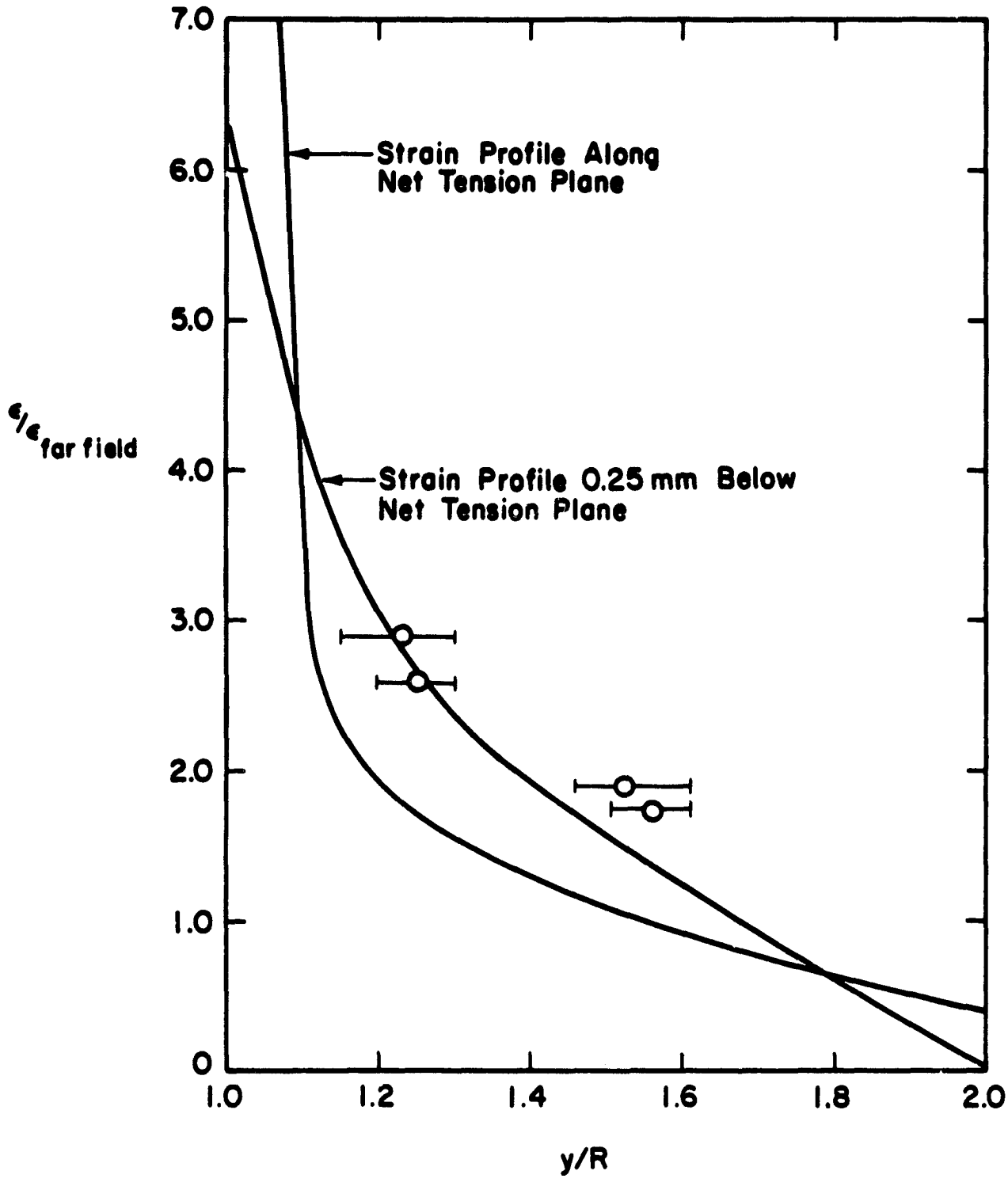

Figure 5. Plot of the Strain Profile for σ_y Along the Net Tension Plane

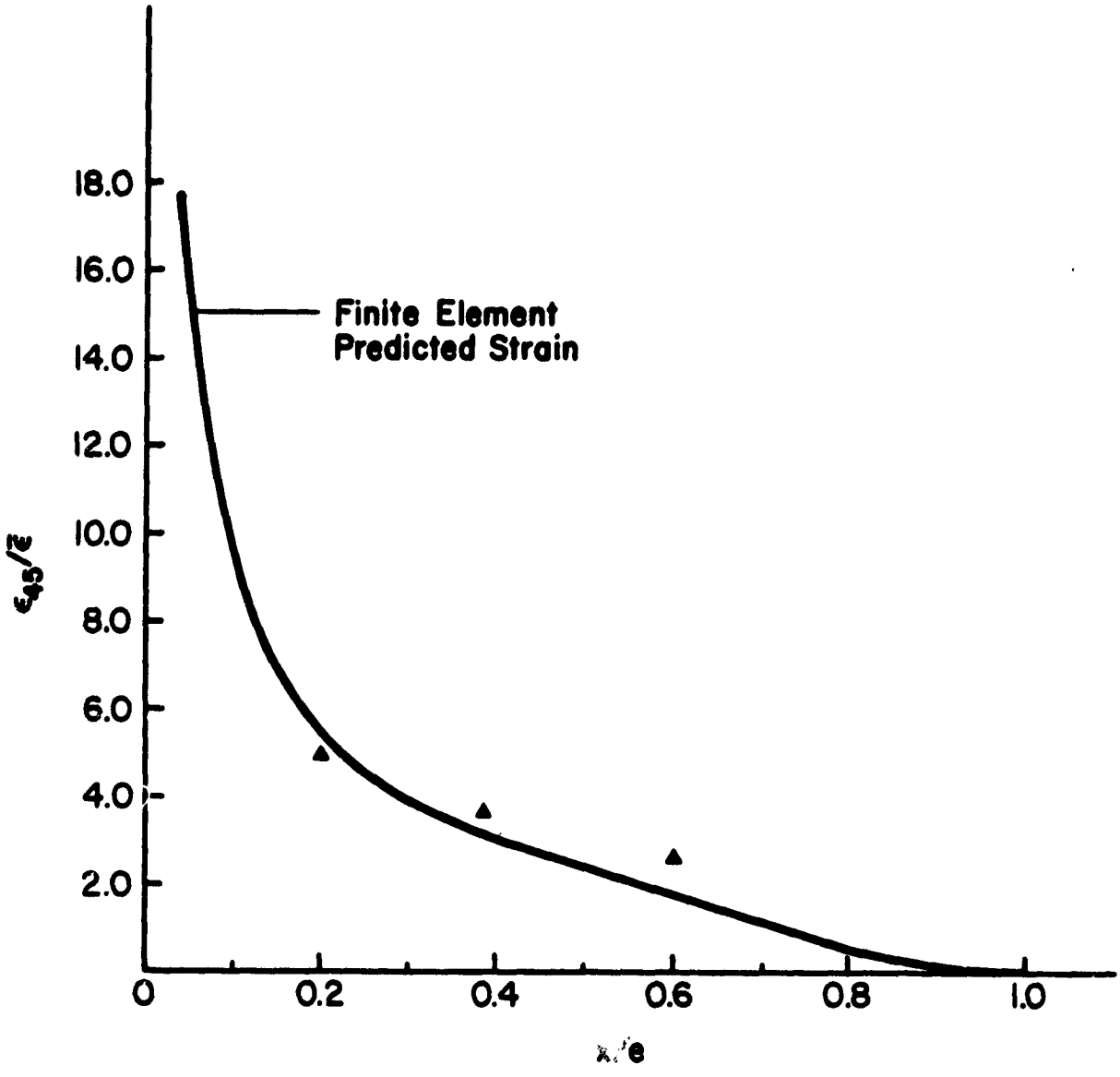

Figure 6. Plot of the Strain Profile Along the Shearout Plane for Strains Oriented at 45° to the Loading Direction

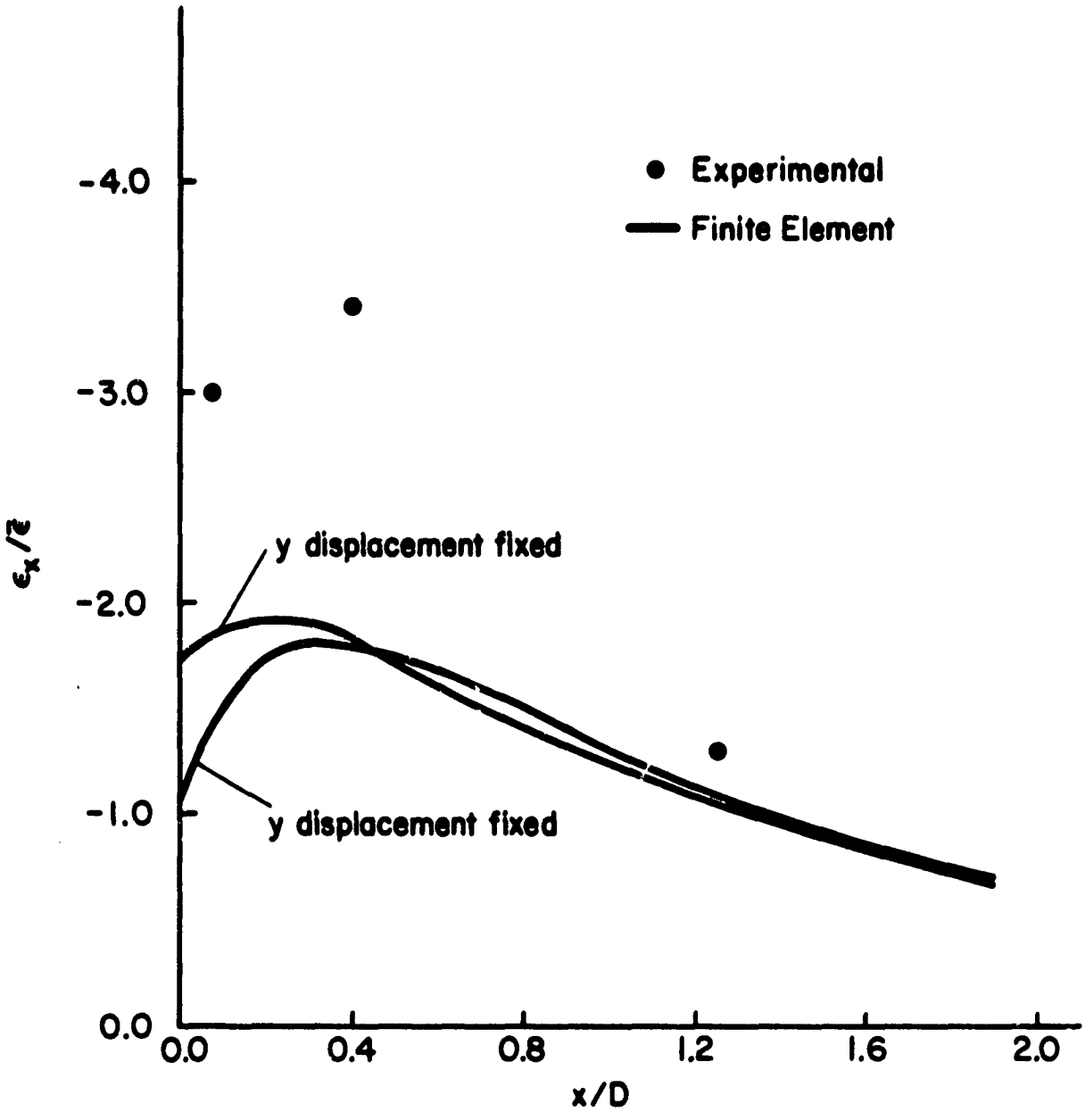

Figure 7. Plot of Bearing Strain σ_x Along the Bearing Failure Plane

interaction. The poor agreement of the bearing data with the finite-element results diminishes confidence in the ability of the model to describe the bearing stresses. Excellent agreement for the net tension and shearout cases verified the accuracy of the model for these two cases in regions removed from the bolt hole.

Failure Criterion Development

Based on observed experimental characterization of bolted joint behavior a "point stress" failure criterion [22,23,24] was applied to the net tension and shearout failure modes while the Tsai-Wu criterion [25] was used for the bearing mode. The "point stress" criterion developed by Whitney for tensile strength of a notched laminate is based on the stress distribution adjacent to the notch. The criterion states that failure occurs when the stress at some critical distance, "d_o", from the edge of the notch reaches the unnotched laminate strength. The failure criterion as applied to the net tension and shearout failure regimes in bolted joints is illustrated graphically in Figures 8 and 9. Only the stress component primarily responsible for failure in the particular mode under consideration is used in the "point stress" criterion. Thus the tensile stress distribution $\sigma_y(x)$ across the net tension plane of the fastener is applied in the net tension failure mode while the shear

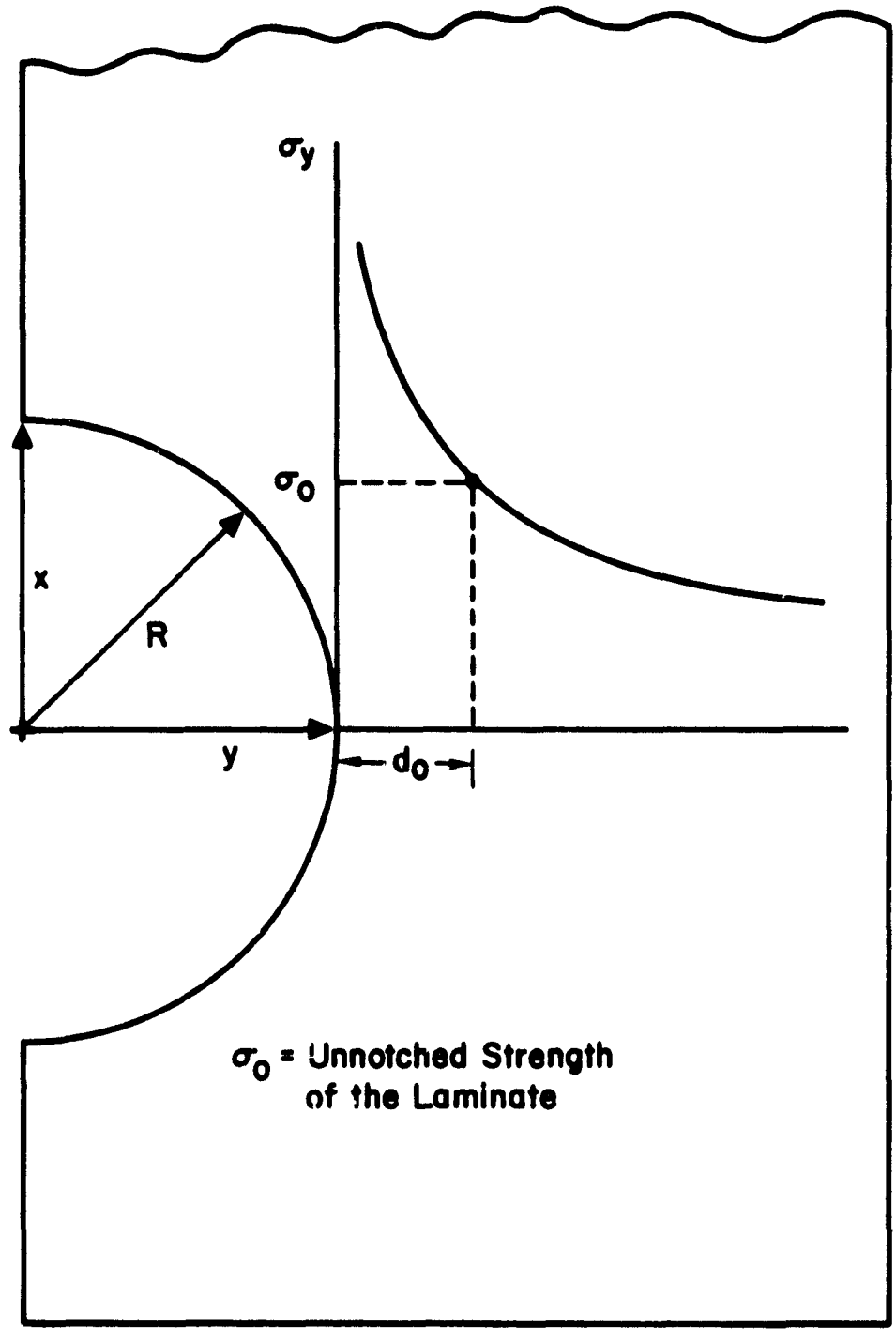

Figure 8. Description of the Net Tension Point Stress Failure Criterion

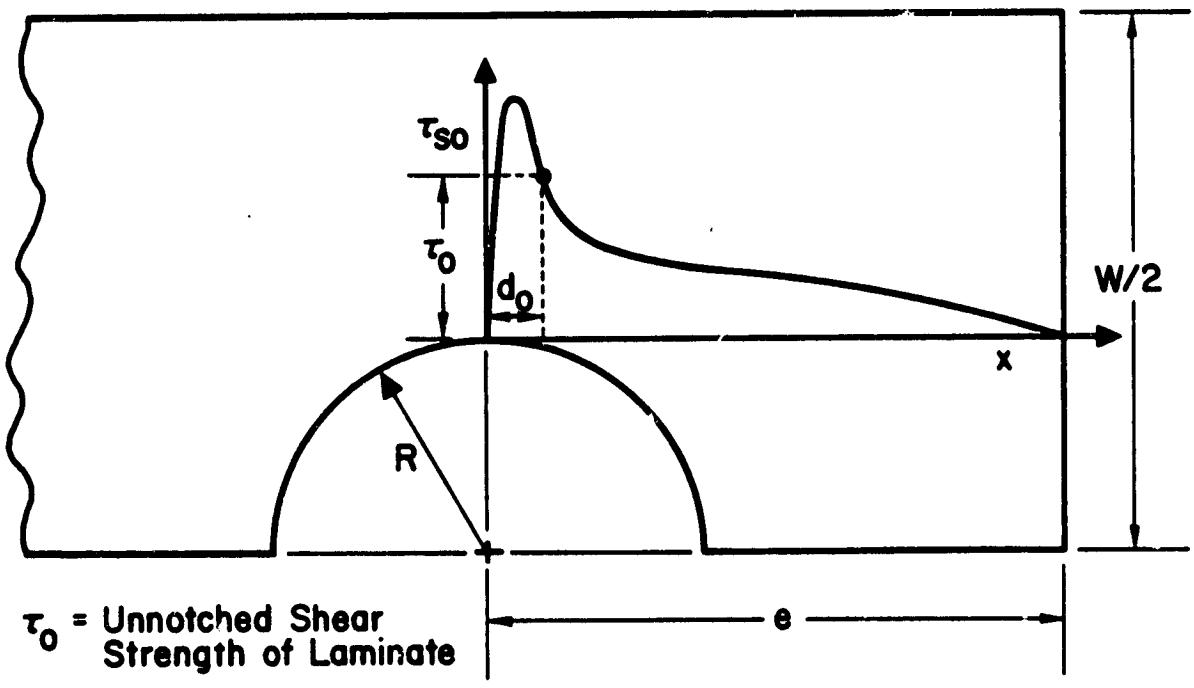

Figure 9. Description of the Shearout Point Stress Failure Criterion

stress distribution, $\tau_{xy}(y)$ along the shearout plane is used for the shearout mode.

The Tsai-Wu failure criterion may be expressed in the following form to predict strength of composites subjected to multiaxial states of stress,

$$F_i\sigma_i + F_{ij}\sigma_i\sigma_j \geq 1$$

where F_i and F_{ij} are strength tensors of 2nd and 4th rank, and the σ_i are usual contracted notation for stress components. The strength tensors must be determined by experiment for each material system considered. Specifically, the strength tensors are defined as follows.

$$F_1 = \frac{1}{X_t} + \frac{1}{X_c}$$

$$F_{11} = -\frac{1}{X_t X_c}$$

$$F_2 = \frac{1}{Y_t} + \frac{1}{Y_c}$$

$$F_{22} = -\frac{1}{Y_t Y_c}$$

$$F_6 = 0$$

$$F_{66} = \frac{1}{S^2}$$

where

X_t = laminate tensile strength in the load direct.

X_c = laminate compressive strength in the load direct.

Y_t = laminate tensile strength transverse to the loading axis.

Y_c = laminate compressive strength transverse to the loading axis

S = inplane shear strength of the laminate

The quantity F_{12} cannot be measured by uniaxial tensile tests but can be measured by a biaxial test. Failure occurs when the sum of the tensor products on the left side of equation 1 equals or exceeds unity.

Implicit in the application of either of the above failure criteria is an analytic representation of the stresses in the joint. Since a closed form solution to the problem is not known, finite element analysis was used to determine the stress profiles.

A simple collocation method was used to fit the stress distributions by polynomial expansions of the space variable in nondimensional form. Net tension stress distributions were fit by a polynomial of the following form:

$$\frac{\sigma_x}{\sigma} = A + B\left(\frac{R}{\bar{Y}}\right)^2 + C\left(\frac{R}{\bar{Y}}\right)^4 + D\left(\frac{R}{\bar{Y}}\right)^6 + E\left(\frac{R}{\bar{Y}}\right)^8 \qquad (2)$$

where the constants A through E were determined by satisfying equilibrium and from points on the finite element stress distribution curve (Fig. 10). Agreement between the finite-element results and the approximate functional representation generated by equation (2) is shown in Figure 10. The shearout stress distribution was modeled by an expression of the form:

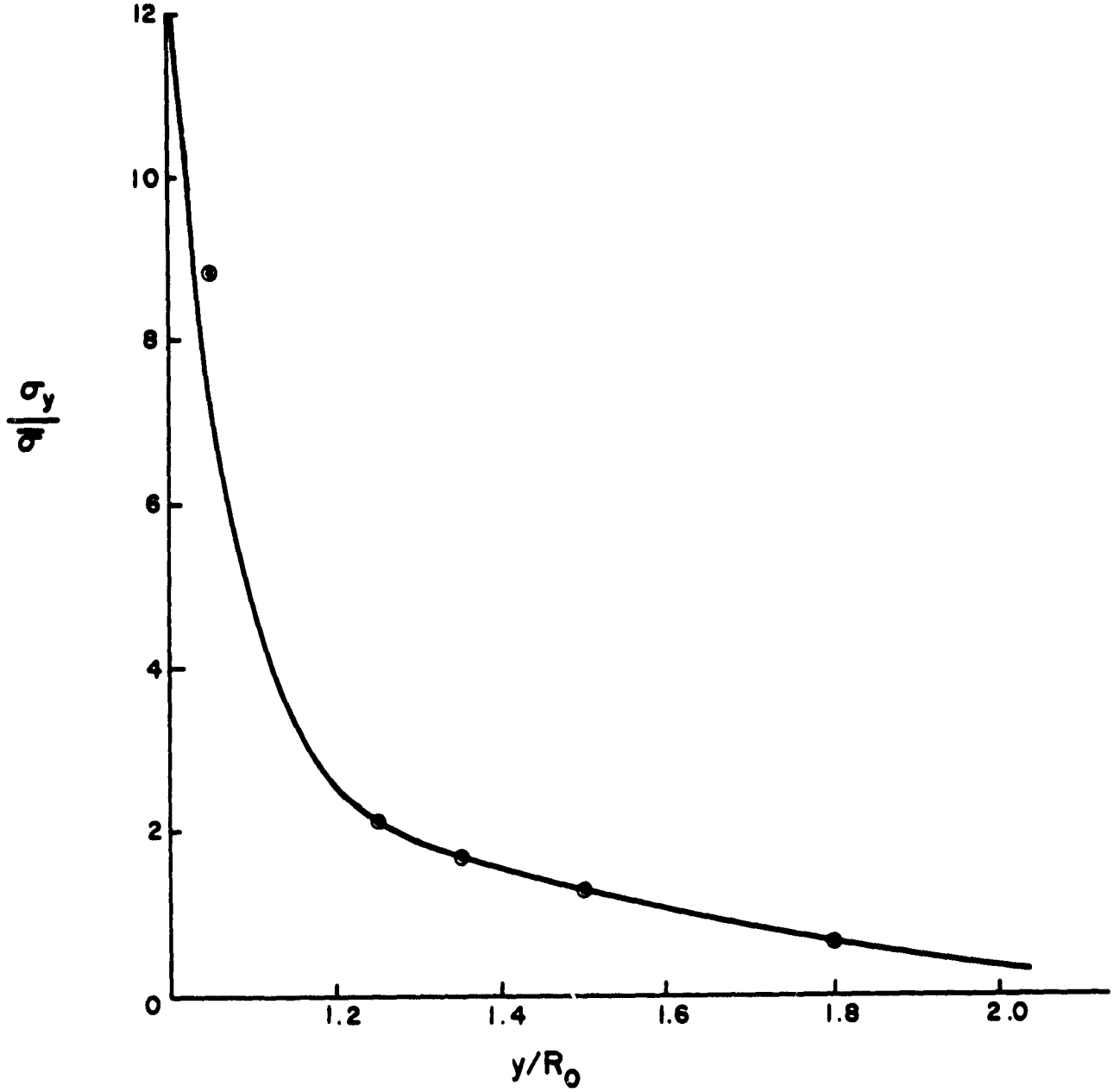

Figure 10. Finite Element Predicted Net Tension Stress Distribution and Comparison to Approximate Polynomial Fit

$$\frac{\tau_{xy}}{\sigma} = A\left(\frac{x_o}{x}\right) + B\left(\frac{x_o}{x}\right)^2 + C\left(\frac{x_o}{x}\right)^3$$

where the constants A, B and C were found by fitting three data points at critical locations on the shear stress distribution curve, Fig. 11. Comparision of the finite element curve with the polynomial approximation shows good agreement in the critical region of high stress concentration near the hole with much poorer agreement in the far field region. The inclusion of higher order terms in the polynomial resulted in the generation of harmonics which induced significant fluctuations in the stresses for small x (near the hole). Only slight increases in accuracy in the functional representation of the stress profile were achieved by the use of more complex functions, and therefore the 3rd order polynomial was considered adequate.

Parametric studies of the net tension and shear stress distributions as functions of the geometric parameters e/D and w/D resulted in the sets of curves in Figures 12 through 14. There was no effect by e/D on the net tension stress distribution while Fig. 12 shows a significant effect of w/D. The shape of the curve describing the stress distribution did not change but was shifted downward with decreasing w/D. Similar effects were noticed for the shear stress distributions. Increasing e/D resulted in a shifting of

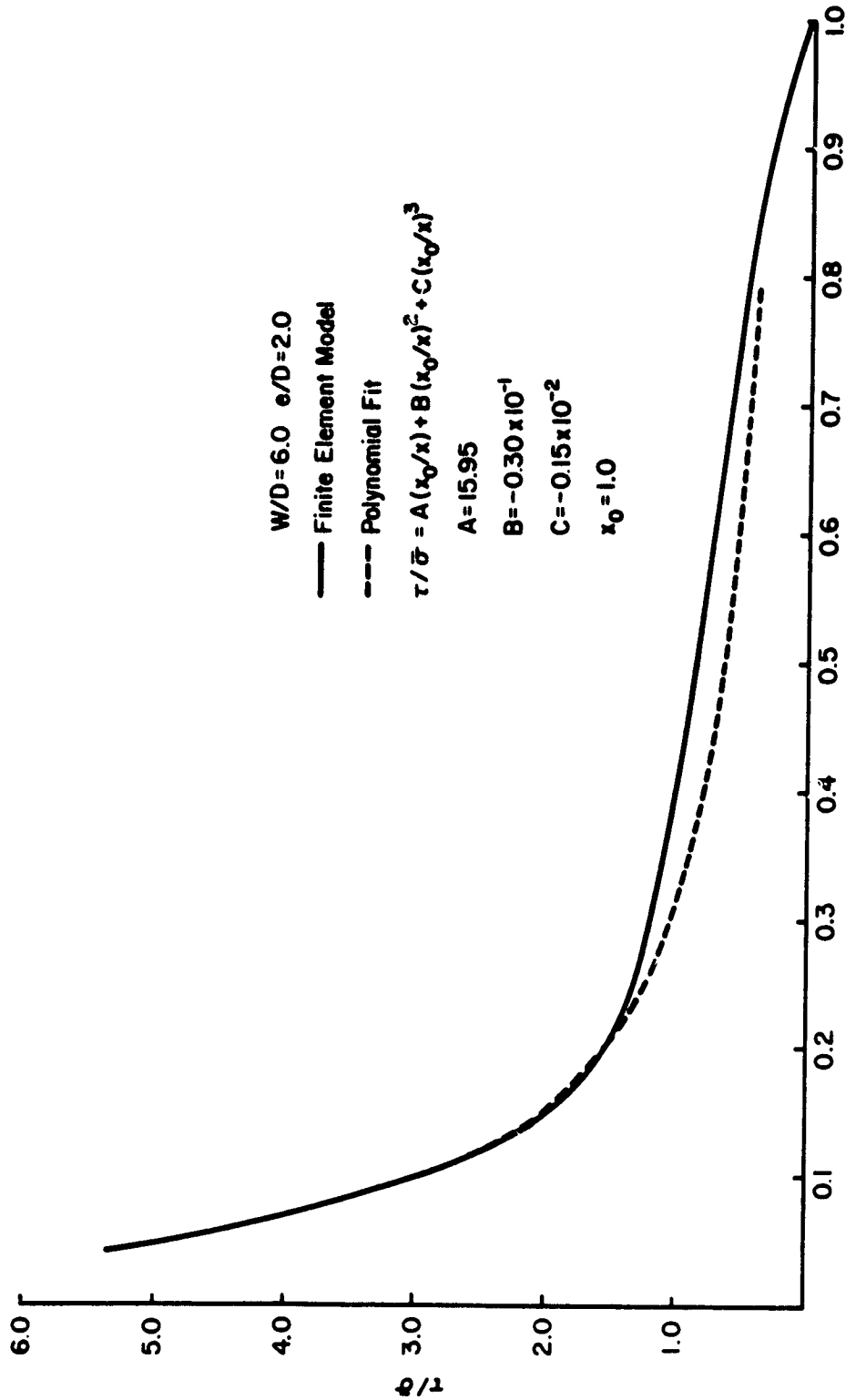

Figure 11. Finite Element Predicted Shearout Stress Profiles and Comparison to Approximate Polynomial Fit

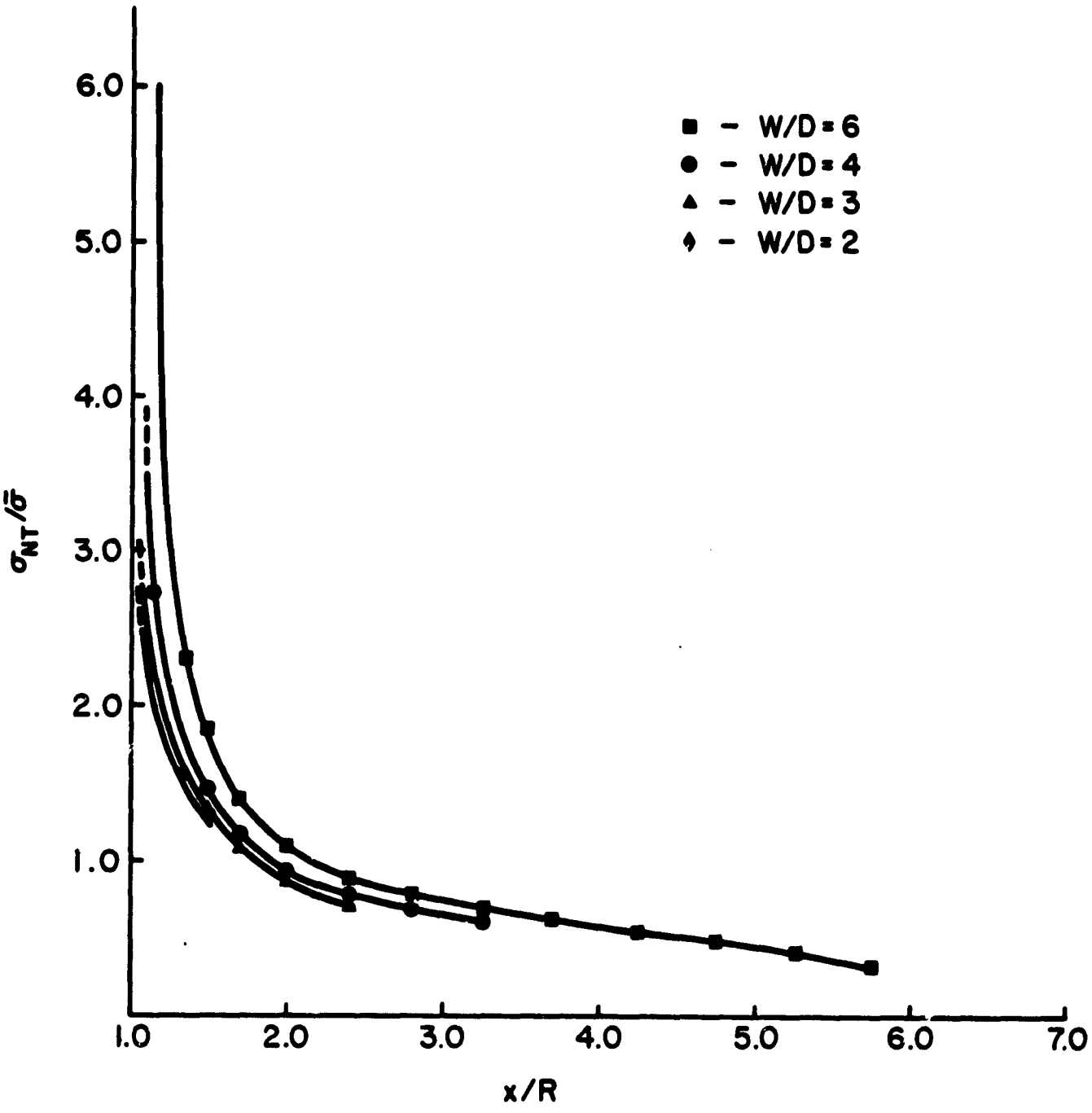

Figure 12. The Effect of Varying W/D on Net Tension Stress Profiles for e/D = 6

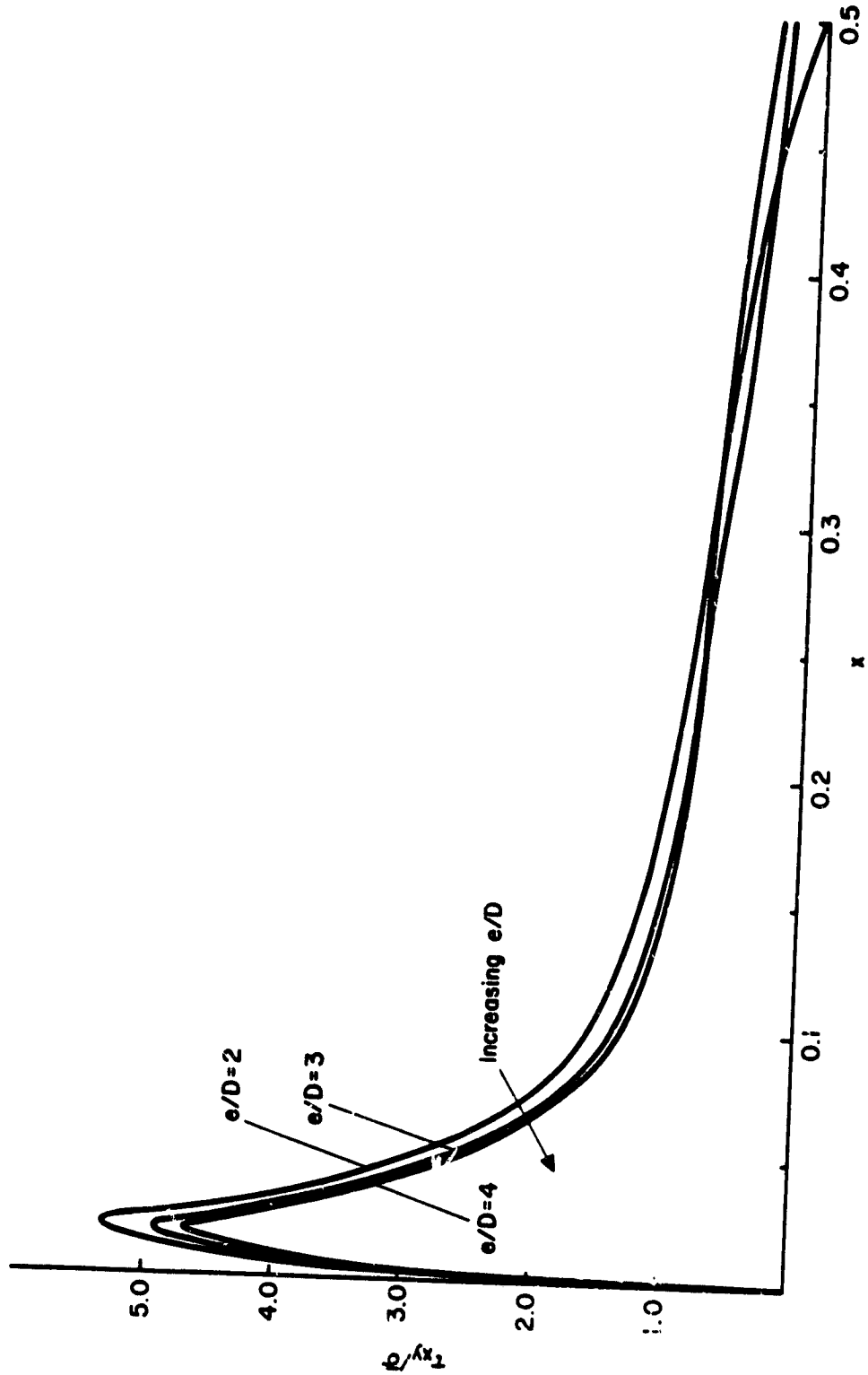

Figure 13. The Effect of Varying e/D on Shearout Stress Profiles for W/D = 6

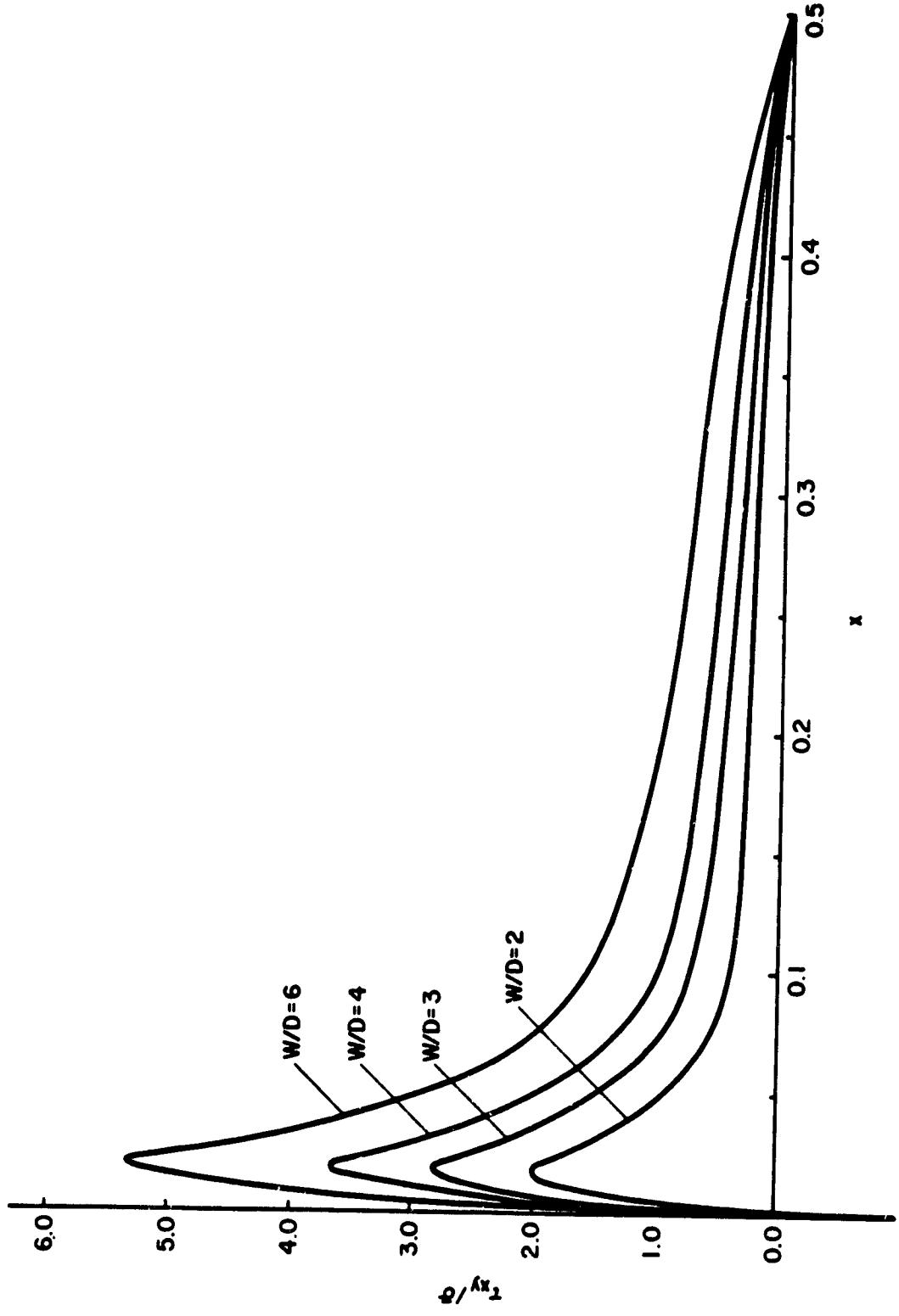

Figure 14. The Effect of Varying W/D on Shearout Stress Profiles for e/D = 2

the curve downward without changing its shape or shifting the location of the maximum stress (Fig. 13). Increases in w/D caused a linear increase in the magnitude of the stresses without changing the shape or location of the curve (Fig. 14). These results for the net tension and shearout stress distributions are better seen by plotting the peak stress versus e/D and w/D as shown in Figures 15 through 17. Non-dimensional parameters were developed from the relationships describing these geometric effects on the stress profiles and used to incorporate the geometric parameters w/D and e/D into the functional stress profile representations. Defining a function ξ (w/D) and fitting the curve in Fig. 15 it is found that

$$\xi(w/D) = 0.956 - 0.044\ \underline{\bar{x}} + 0.089\ \underline{\bar{x}}^{2}$$

where $\underline{\bar{x}} = w/2D$

for the net tension mode. Similarly it can be shown that two parameters $\rho(w/D)$ and $\zeta(e/D)$ can be defined and found to have the following forms derived from the curves in Figures 16 and 17

$$\rho(w/D) = \frac{M \cdot (w/D)}{\tau_{max}\Big|_{w/D=6}}$$

where M = slope of the τ_{max} versus w/D curve in Figure 16 and

$$\zeta(e/D) = 0.75\ e^{(0.5-e/D)} + 0.84$$

for the shearout failure mode.

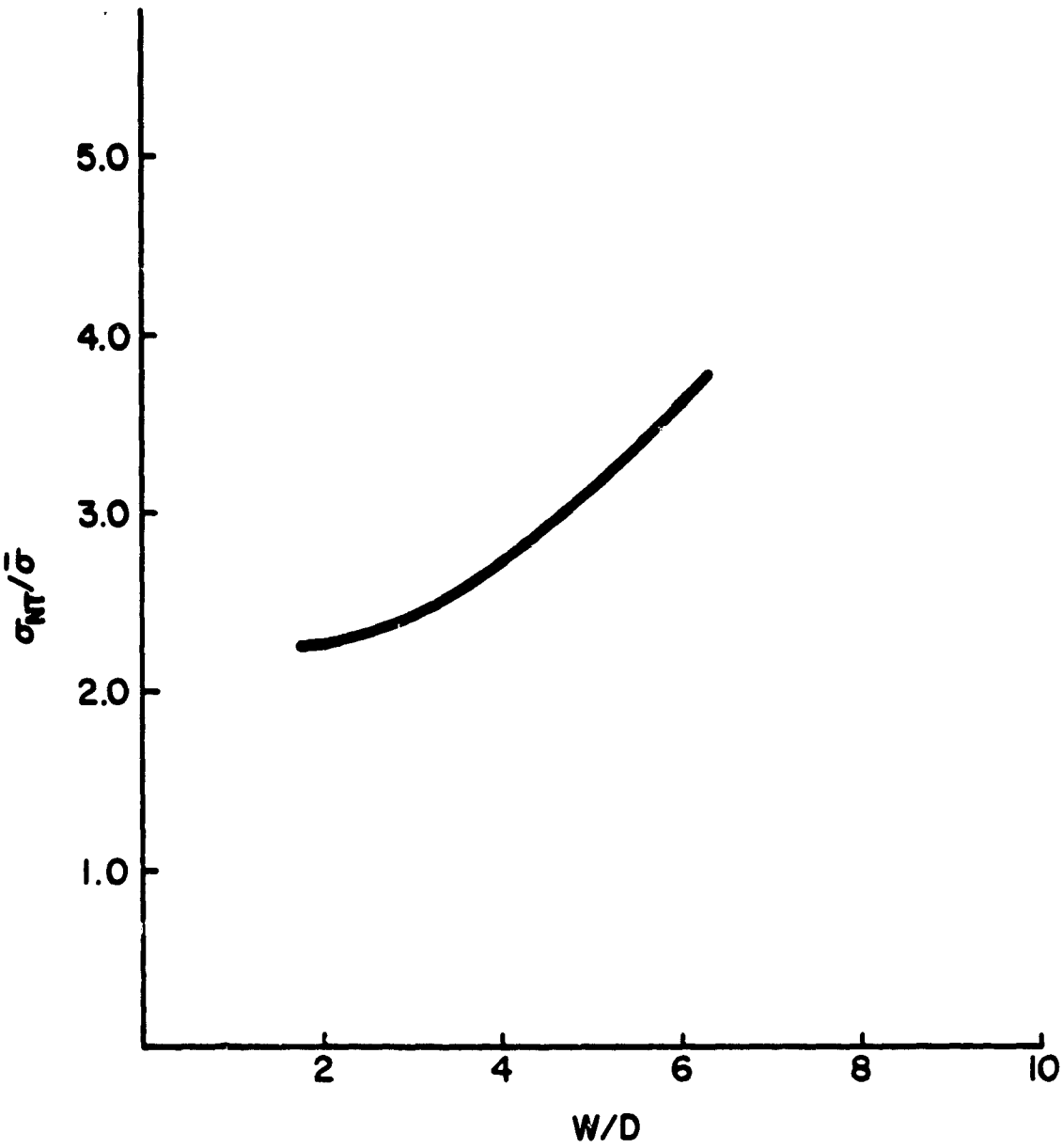

Figure 15. The Variation in Net Tension Stress Concentration with W/D

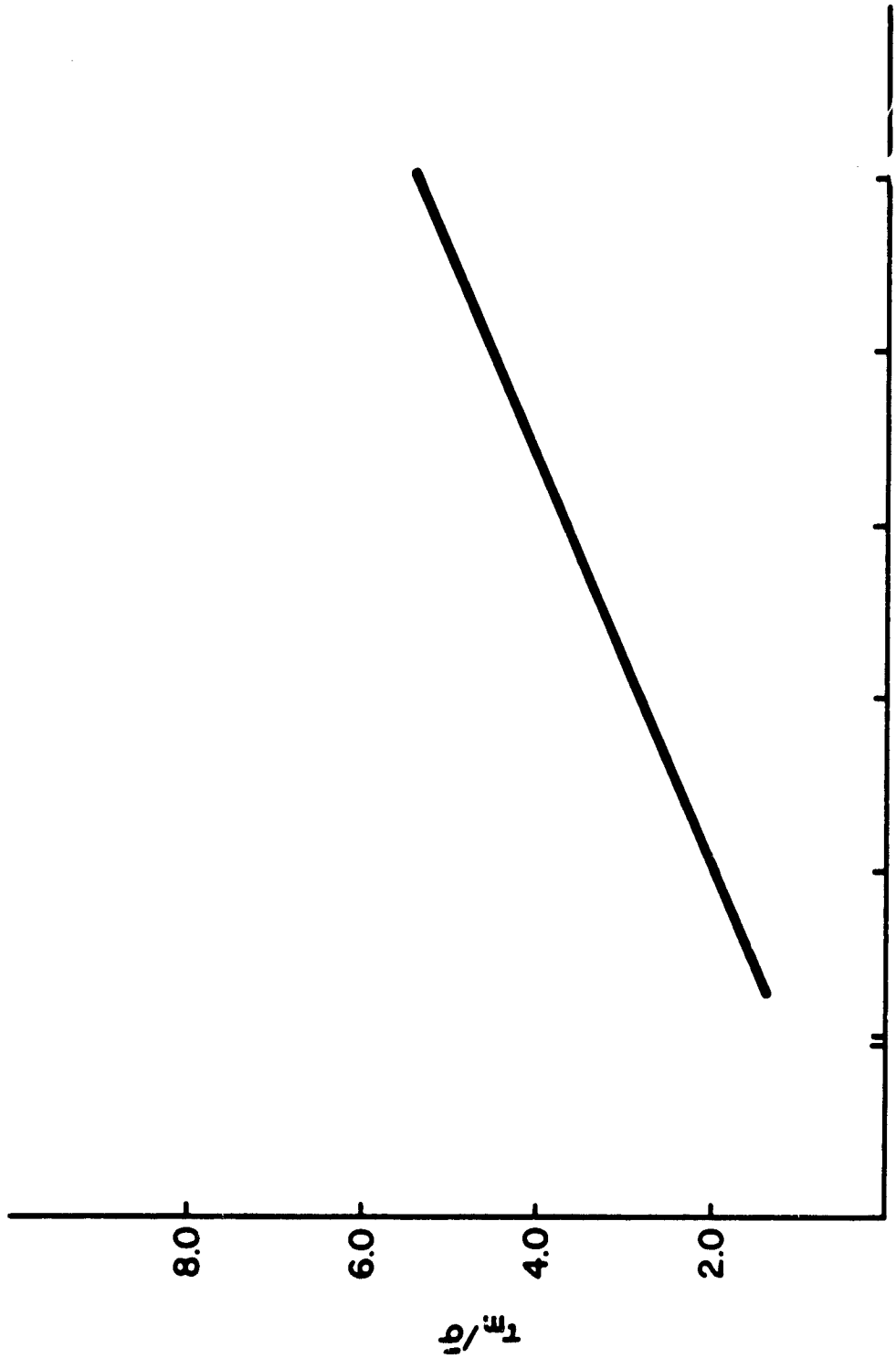

Figure 16. The Variation in Shearout Stress Concentration with W/D

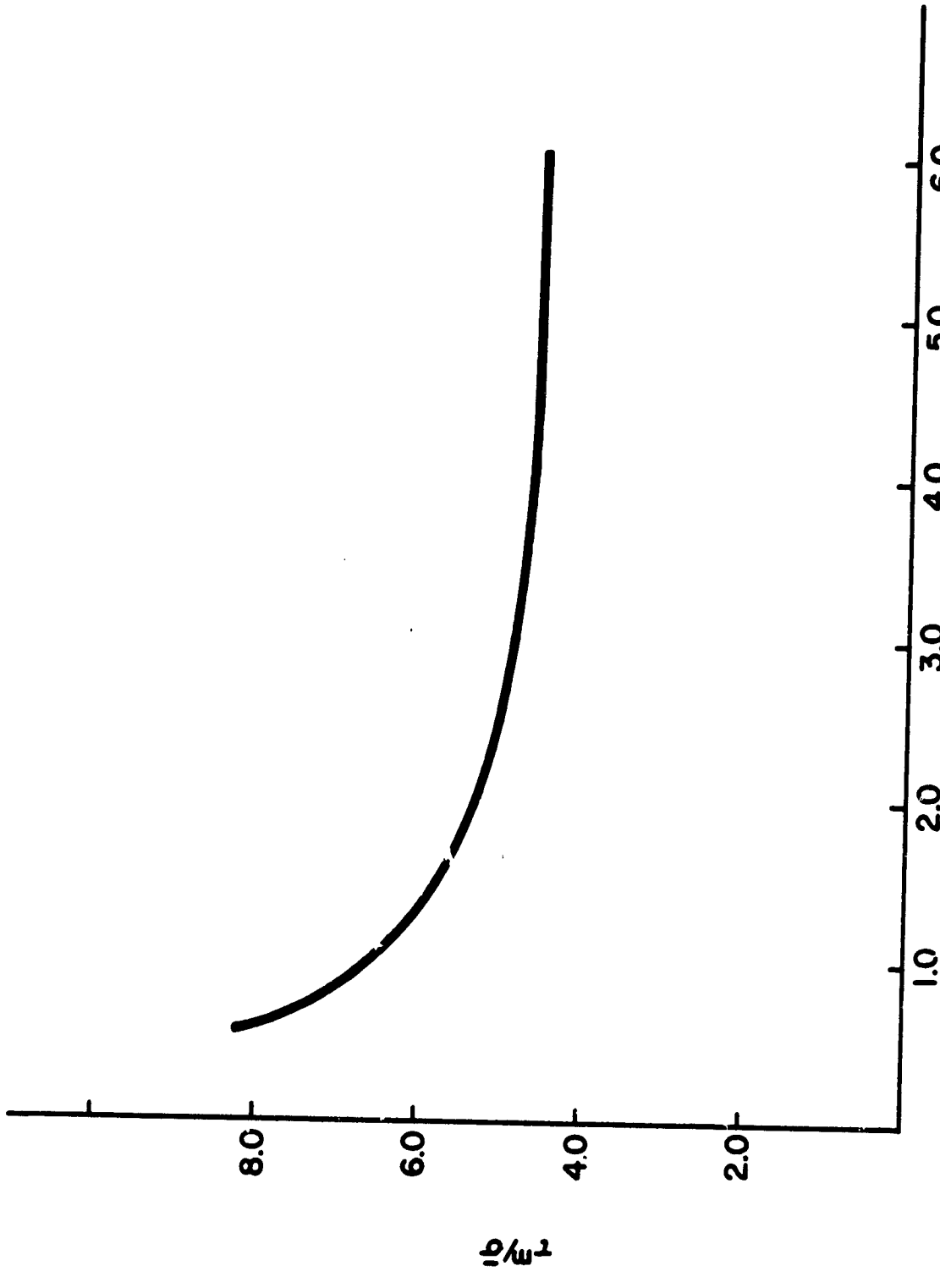

Figure 17. The Variation of Maximum Shear Stress Concentration with e/D

Combining the geometric parameters and the original stress profiles results in functions which describe the stress profile incorporating the geometric effects.

$$\frac{\sigma_{nt}}{\bar{\sigma}} = \xi(w/D)\left[A + B\left(\frac{R}{Y}\right)^2 + C\left(\frac{R}{Y}\right)^4 + D\left(\frac{R}{Y}\right)^6 + E\left(\frac{R}{Y}\right)^8\right]$$

and

$$\frac{\tau_{sa}}{\bar{\sigma}} = \zeta(e/D)\cdot\rho(w/D)\left[A\left(\frac{x_o}{x}\right) + B\left(\frac{x_o}{x}\right)^2 + C\left(\frac{x_o}{x}\right)^3\right]$$

These approximate expressions for the stress are suitable for incorporation into the failure criterion.

The "point stress" failure criterion is expressed as

$$\sigma_x \Big|_{x=d_o} = \sigma_o$$

where

σ_x is the stress component adjacent to the hole for the failure mode under consideration

σ_o is the unmatched strength of the laminate for the failure mode under consideration.

d_o is the critical distance.

The critical distance parameter is a function of hole size and has the following form [22].

$$d_o = \frac{1}{C}\left(\frac{R}{R_o}\right)^m$$

Constants C and m are found from empirical data by finding d_o

for two notch sizes. This was carried out for both failure modes with different resultant m and C values. The values of m and C for the net tension failure mode were 0.83 and 8.30, respectively, while for the shearout failure mode m was 0.140 and C was 7.12.

The bearing mode failure criterion considers the effects of all in-plane stress components in the compressive region of the joint. Each stress component σ_x , σ_y and τ_{xy} are plotted in Figure 18 from the centerline of the hole's edge along the y-axis. It is apparent that the maximum compressive stress σ_x does not occur at the centerline but very slightly off the centerline. This must be considered when applying the Tsai-Wu failure criterion.

Parametric studies evaluating the effects of geometry on the bearing stress profiles are summarized in Figures 19-22. The plane stress finite element analysis shows that increasing w/D results in increasing compressive stress and a change in the distribution of the stress (Fig. 19). Similarly Fig. 20 shows that increasing e/D results in increasing stresses and slight changes in their distribution. This same information is represented in a more convenient form by Figures 21 and 22. Notice that the maximum predicted compressive stress is less than half that of the stress calculated

for the projected pin bearing area. This leads to further suspicion that two-dimensional, plane-stress analysis does not accurately predict the stresses in the bearing region.

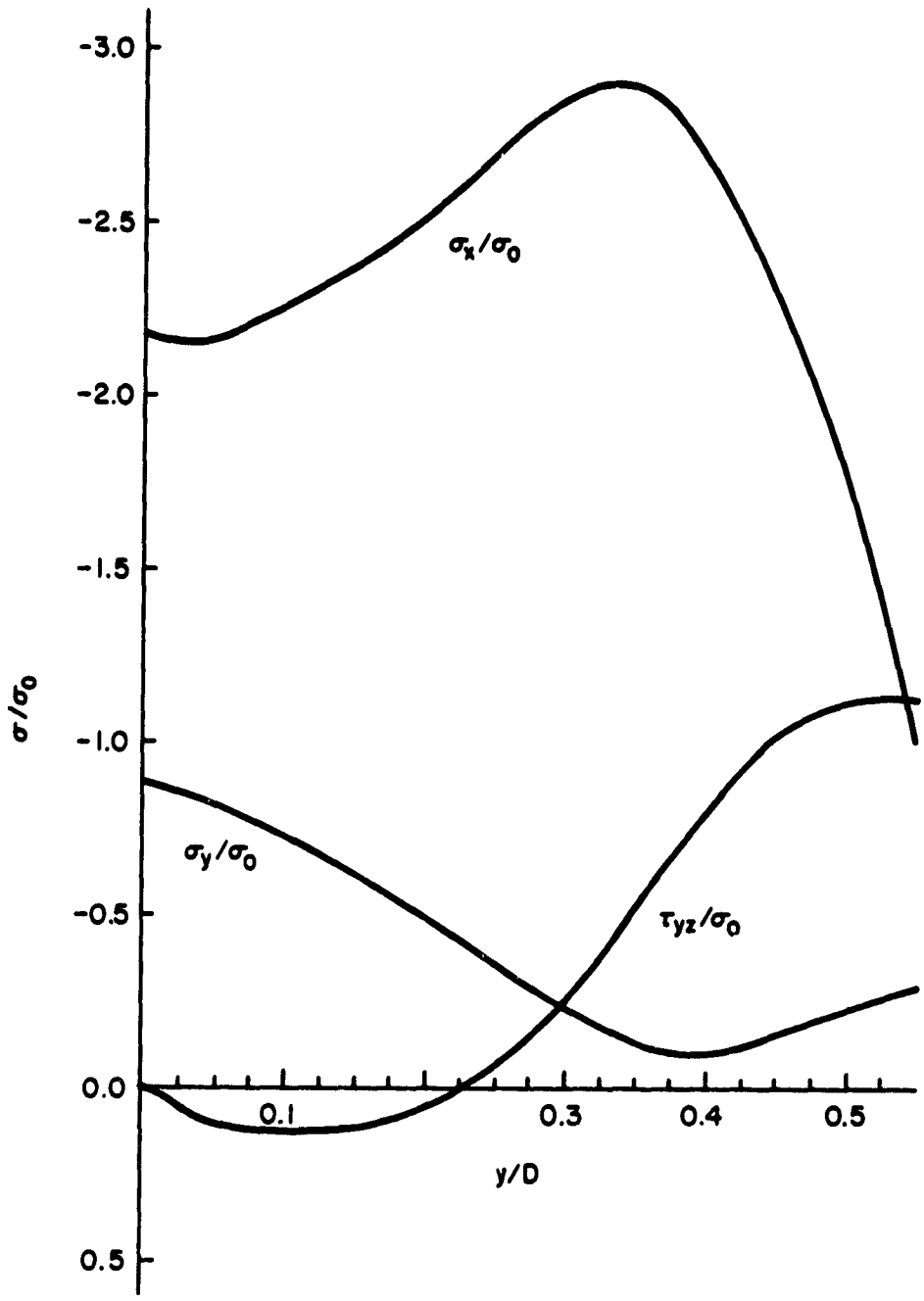

Figure 18. Variation of Stress Components in the Vicinity of the Bolt Hole

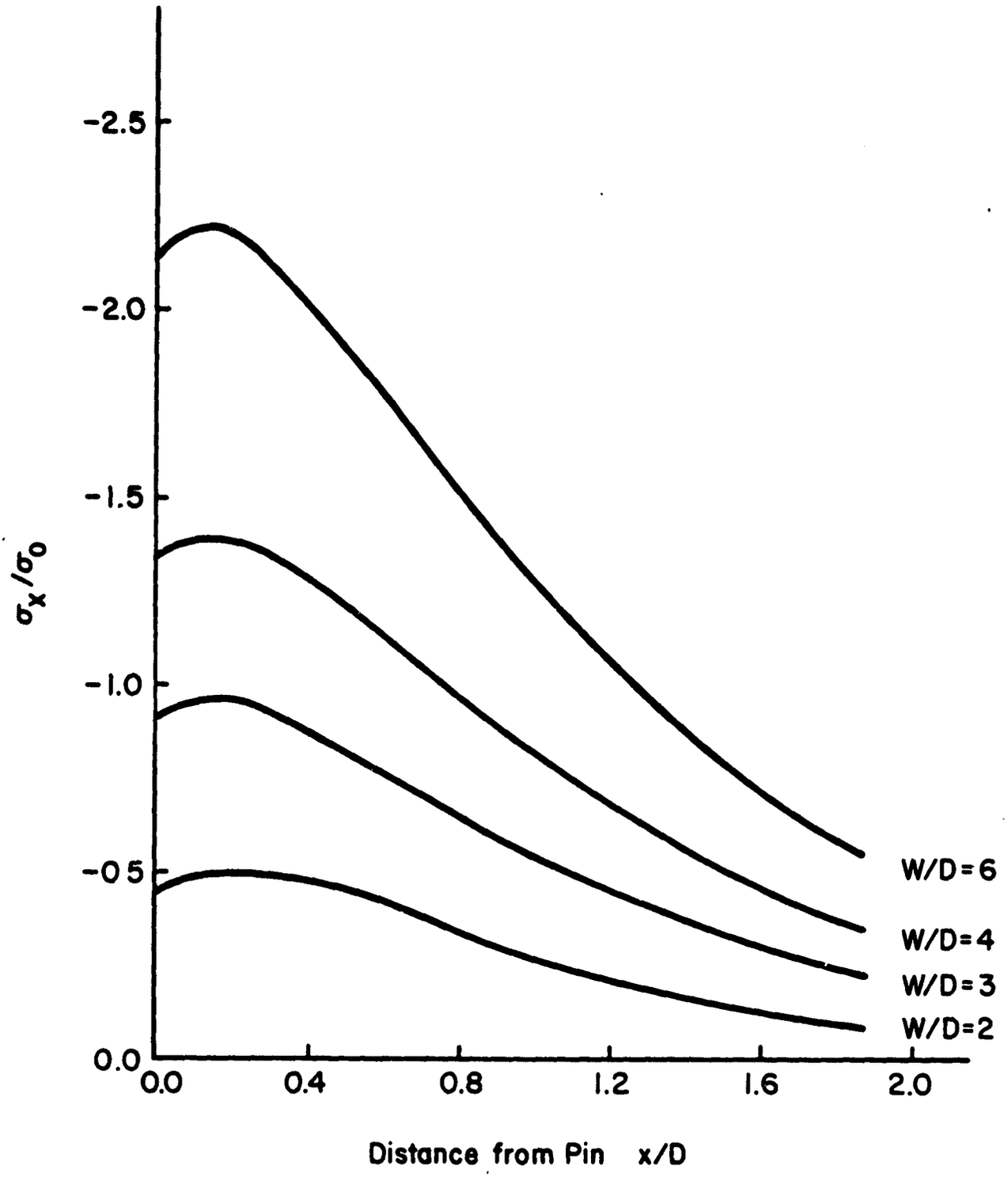

Figure 19. Compressive Stress Distribution Along Joint Centerline as a Function of W/D

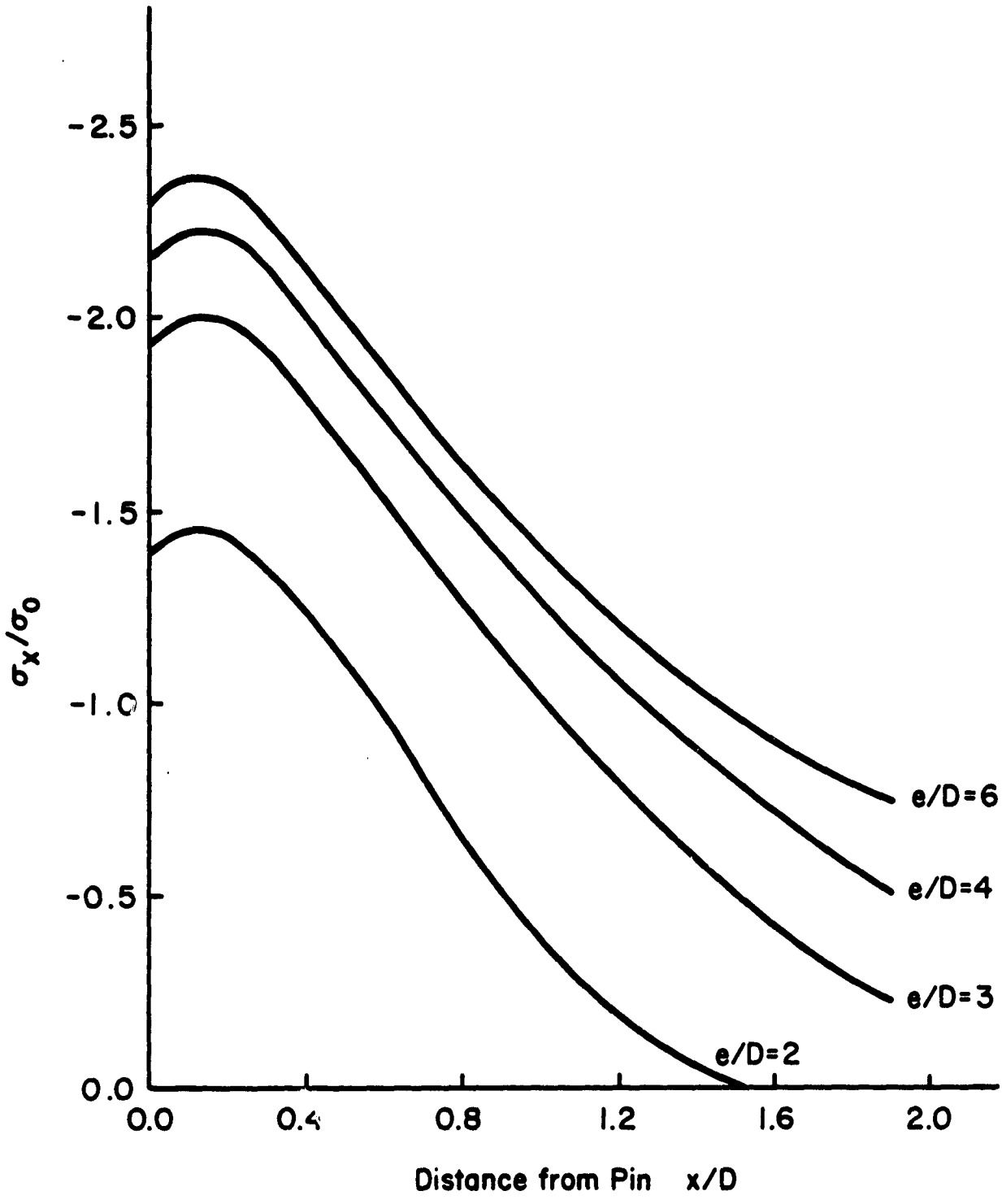

Figure 20. Compressive Stress Distribution Along Joint Centerline as a Function of e/D

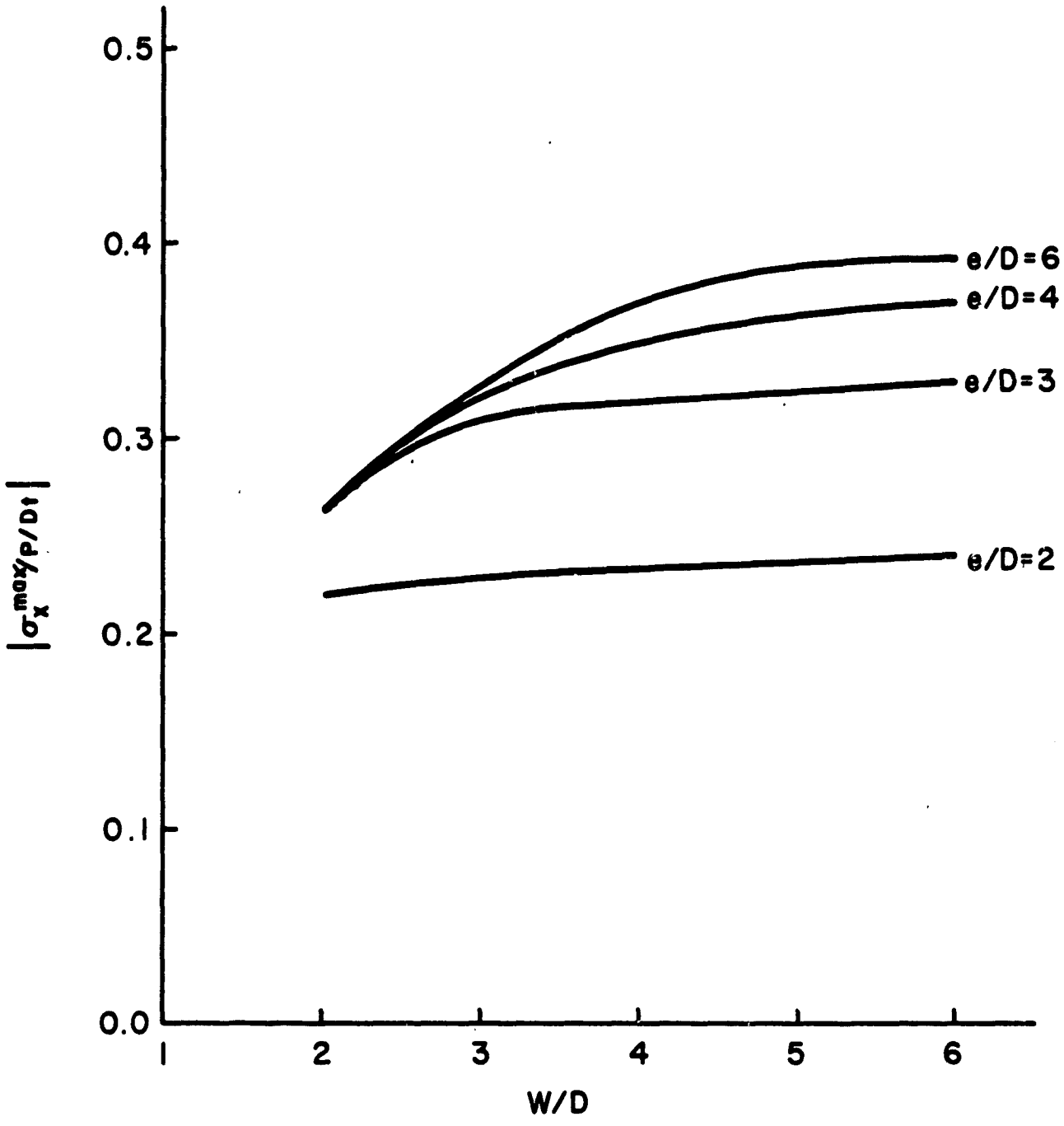

Figure 21. Maximum Compressive Stress Along Joint Centerline as a Function of W/D

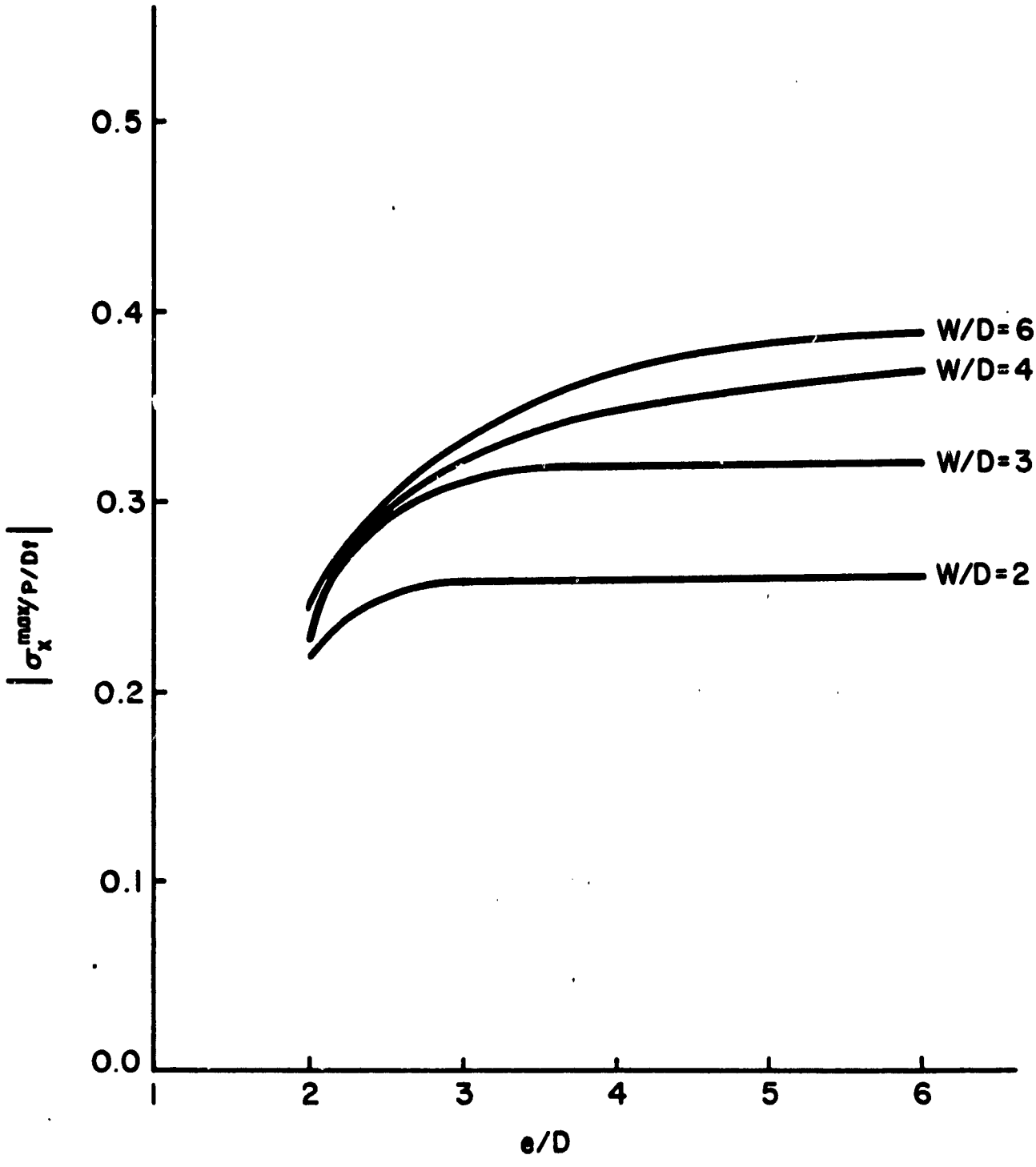

Figure 22. Maximum Compressive Stress Along Joint Centerline as a Function of e/D

RESULTS AND DISCUSSION

The experimental data from the fastener, hole size study are reported in tabular form in Appendix A. For the limited range of fastener sizes investigated the effect was small. The net tension failure exhibited slightly decreasing strength with increasing hole diameter. Shearout failures resulted in the opposite trend, increasing strength with increasing hole size. Bearing failures showed no hole size effect at all.

The hole size effects for the net tension and shearout modes were incorporated into the failure model through d_o . In Figures 23 and 24 failure curves were calculated using the derived failure criteria for a range of fastener sizes while holding w/D and e/D constant. The excellent correlation found between the experimental data and the analytical results for both failure modes occurs because two of the three data points were used in the determination of constants in the failure model and thus is not surprising. Since the hole size effect is small, the predicted behavior should remain accurate for the range of fastener sizes of practical interest.

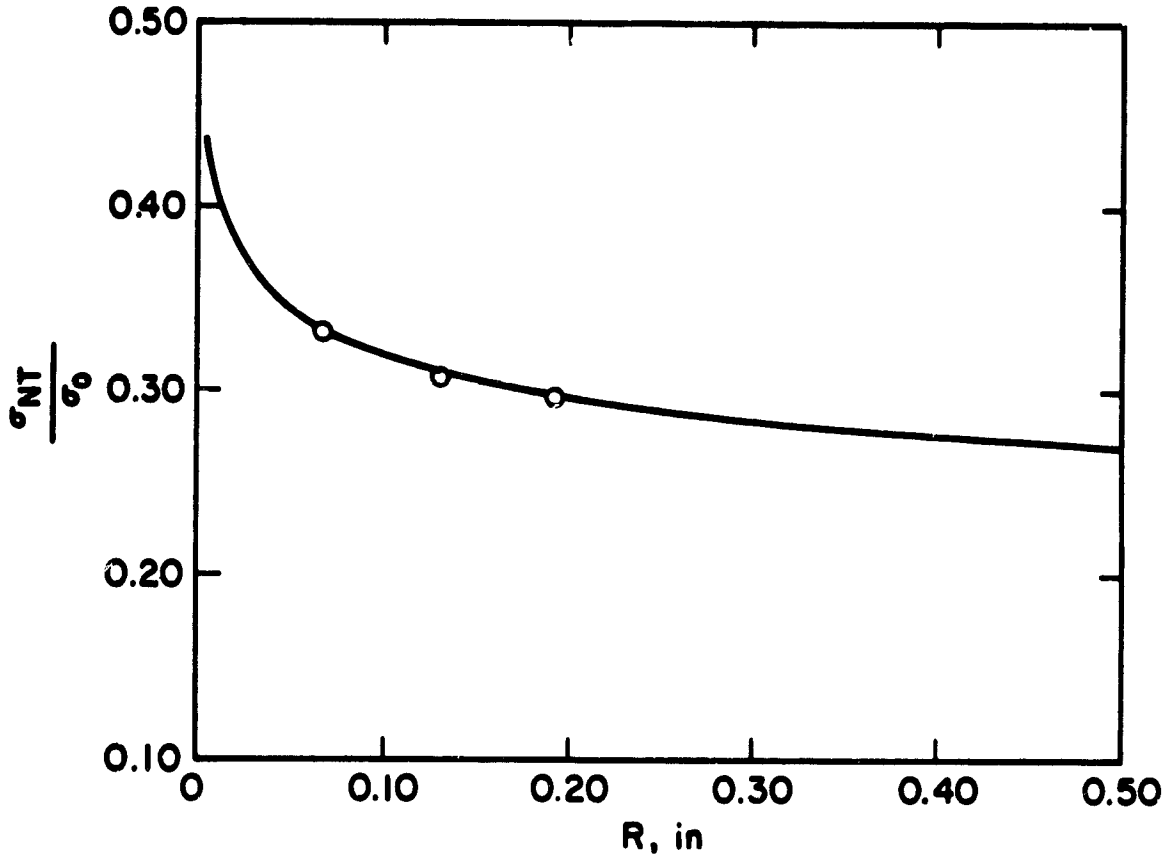

Figure 23. Correlation of Model Predicted Net Tension Strengths with Experimental Data as a Function of Hole Diameter

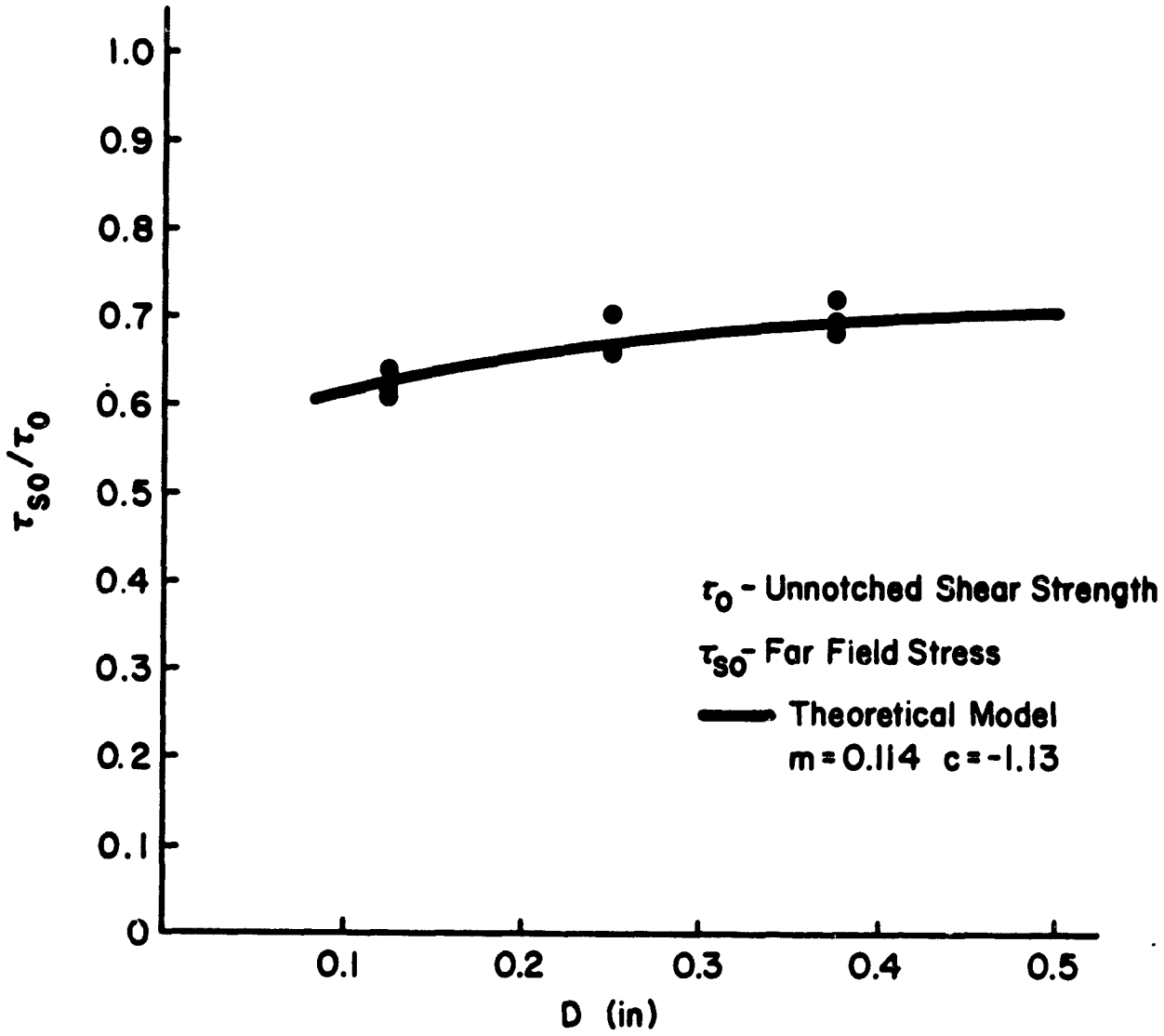

Figure 24. Correlation of Model Predicted Shearout Strengths with Experimental Data as a Function of Hole Diameter

From previous test programs [15,9] data was available to investigate the accuracy of the newly developed failure criteria in predicting net tension and shearout failure strength for several w/D geometries. In Figure 25 the solid curves are the predicted failure surfaces for two distinct fastener sizes for the net tension mode. The circular symbols represent data from the current test program. The triangular symbols are data from Hartsmith [2] for a similar laminate but from a different graphite-epoxy system (Narmo 5208/T300). The agreement between the experimental data and the predicted failures is excellent. Similar results were found for the shearout failure mode as seen in Figure 26.

Bearing failure analysis was attempted using the Tsai-Wu strength criterion. For convenience the joint geometry was redefined in polar coordinates as shown in Figure 27. The Tsai-Wu criterion was applied to the laminate at each element location on the hole boundary between the angular positions $\theta = 0°$ and $90°$. The state of stress at failure was determined by setting the finite-element far field stress input equal to the far field stress experiment for bearing failure. This set of stress components obtained were then used as input to the Tsai-Wu criterion to test its validity for bearing failure analysis.

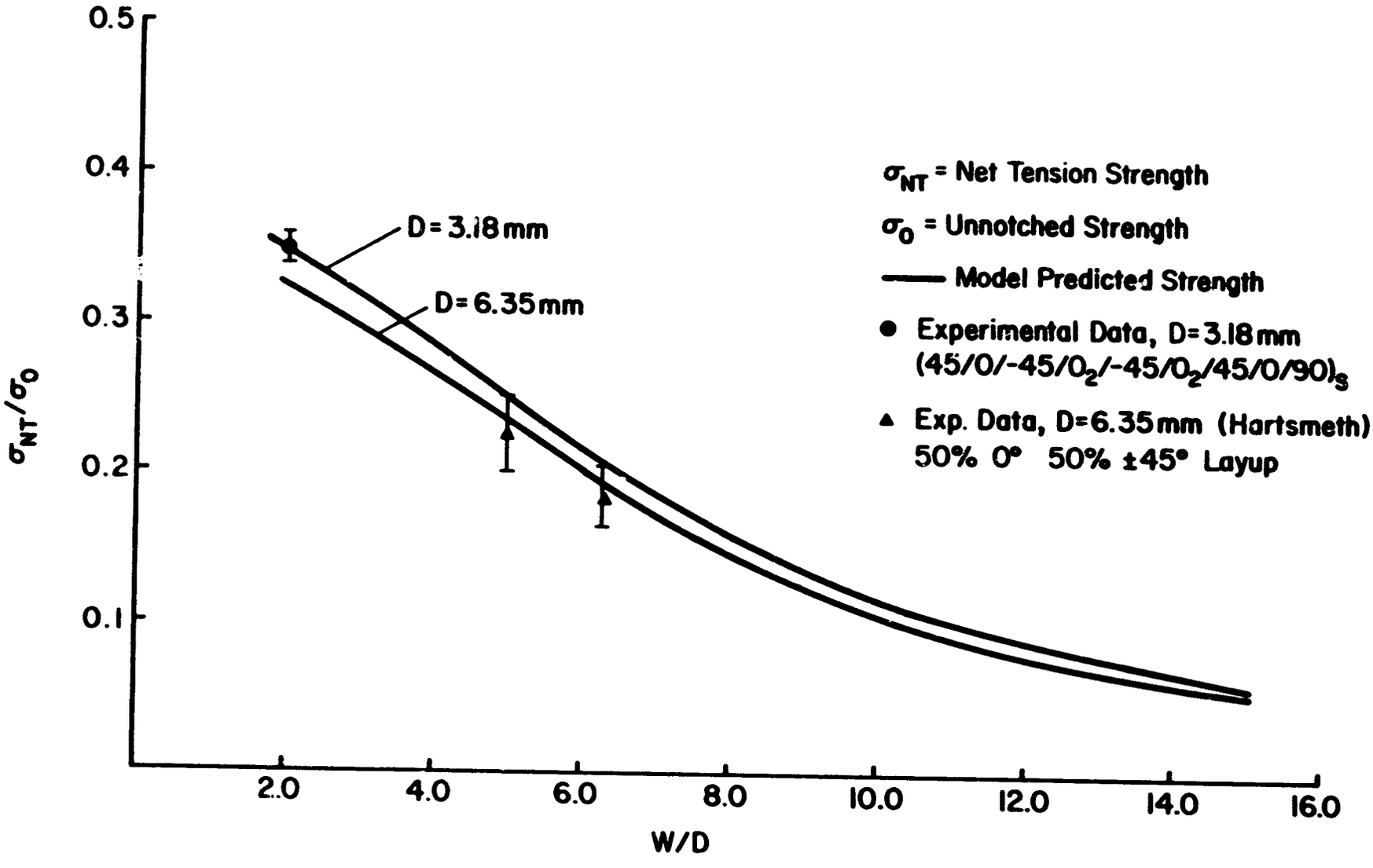

Figure 25. Correlation of Net Tension Strength as a Function of W/D with Experimental Data

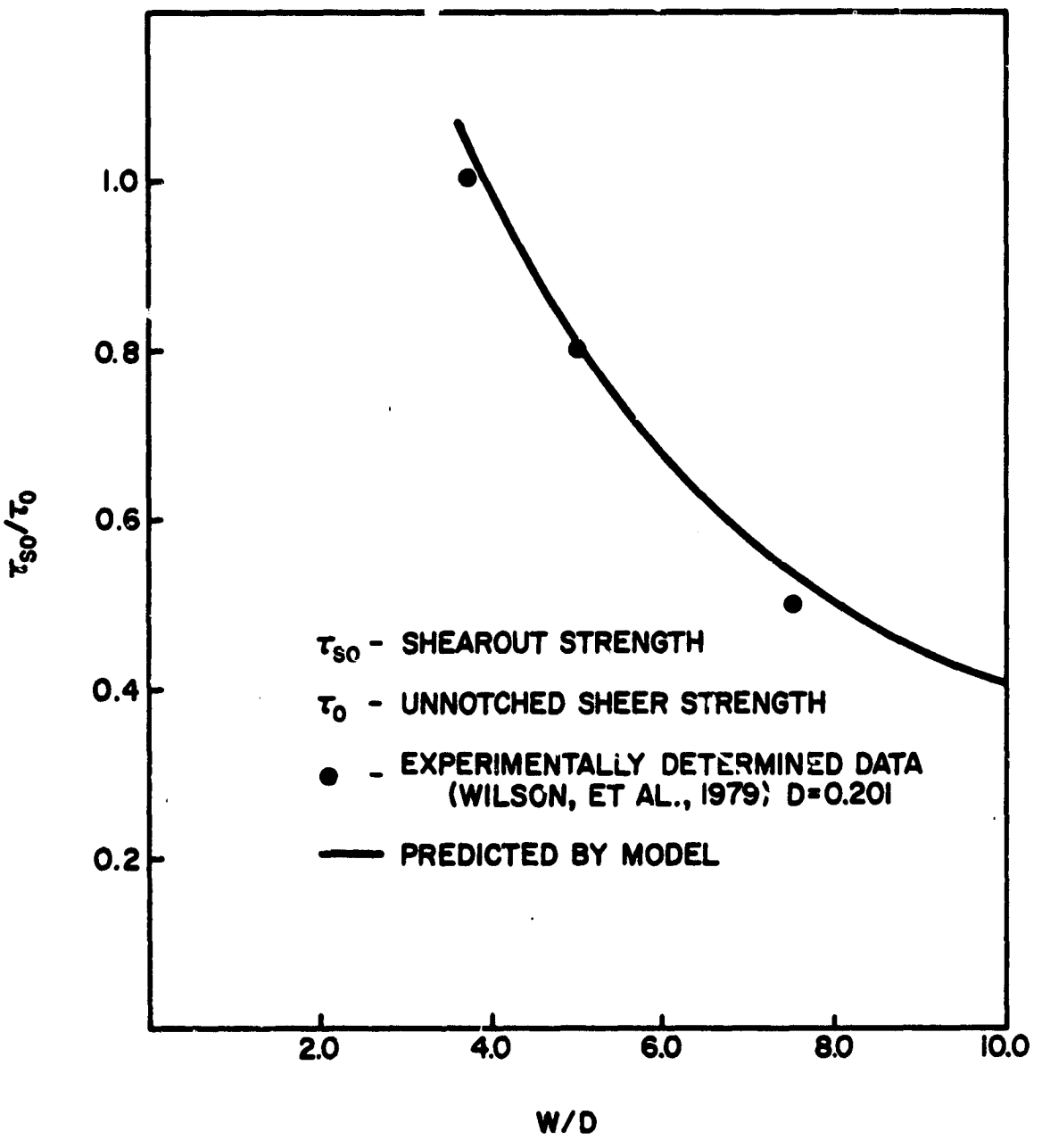

Figure 26. Correlation of Shearout Strength as a Function of W/D with Experimental Data

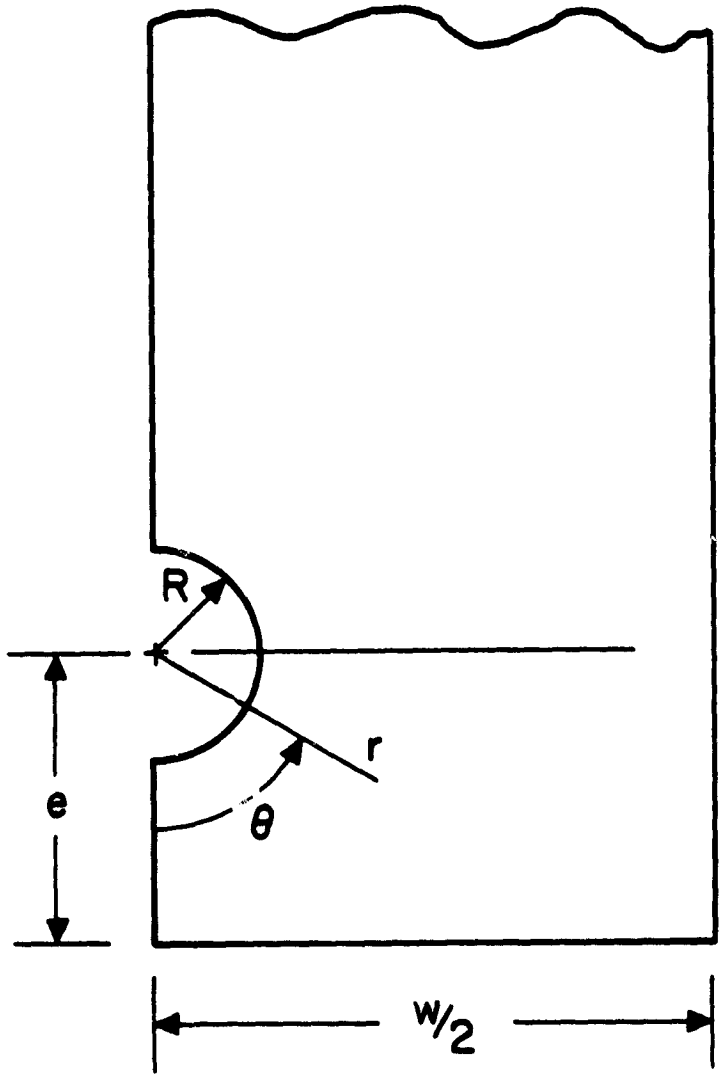

Figure 27. Polar Coordinate Geometry Introduced for the Bearing Failure Analysis

The Tsai-Wu criterion predicted strength was seen to increase monotonically with increasing angular position in the 0° to 45° range while developing an exponential character and increasing without bound as the 90° position was approached. This behavior presented a problem in interpretation of results since the bearing load reacted by the laminate decreases as the 90° position is approached. Since the 0° to 45° interval reacts most of the bearing load which causes failure ahead of the fastener this region was selected as the valid region for application of the criterion. The maximum value of the criterion in this region was 0.5 at the 0°±45° location when the "failure stress components" were input. This value is significantly different from the value of approximately 1.0 expected at failure and is non-conservative.

One possible explanation for the poor results can be linked to the plane stress finite element analysis. The plane stress assumption for the bearing analysis is not a good approximation. This was verified for the pin bearing case where measured strains were much greater than predicted strains. The interlaminar stress components σ_z , τ_{xz} , and τ_{yz} could significantly affect the compressive strength of the laminate. Another factor which affects the results is fastener torque and washer size. According to Stockdale and Matthews [26] in Figure 28 a twofold increase

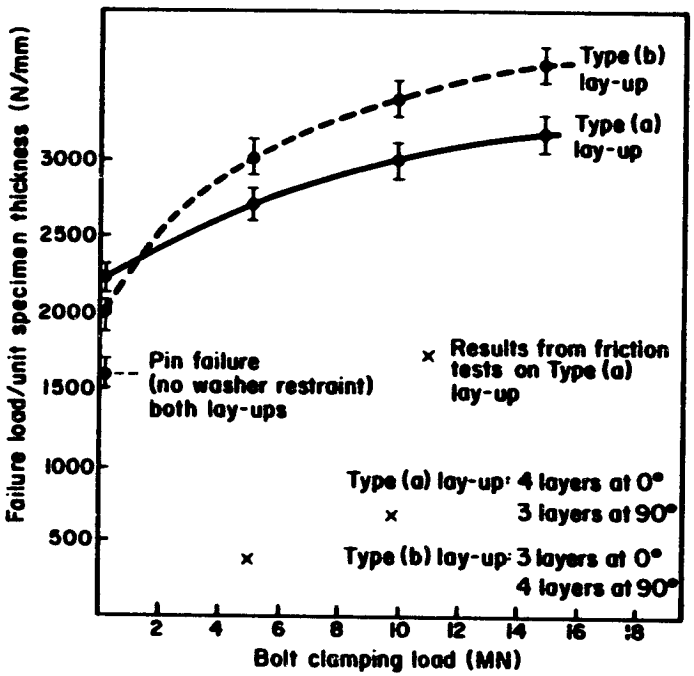

Figure 28(a). Effect of Fastener Torque on Bearing Strength

(Stockdale and Matthews [26].)

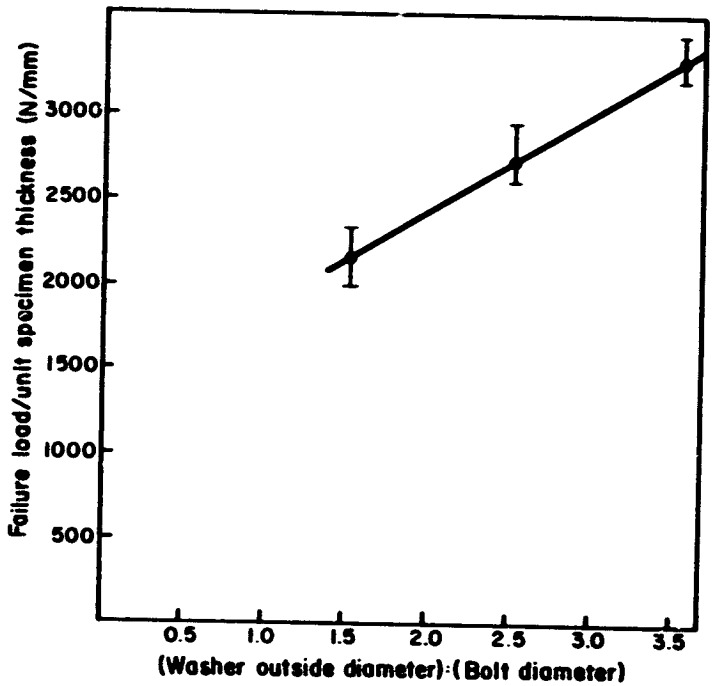

Figure 28(b). Effect of Washer Size on Bearing Strength

in strength can be achieved by increasing the fastener clamping load from finger light to approximately 14 MN. Similarly if the washer diameter is increased from 2 to 4 times the fastener diameter (D) the failure strength exhibits a twofold increase. Thus it is possible that a combination of low torque and small washer area produced low joint bearing strength. A check with the literature appears to refute this hypothesis, however. The bearing strengths which were measured in the present tests compare closely with those of Hartsmith and others [9,10]. With the accuracy of the bearing stress analysis questionable it is not possible to assess the validity of the Tsai-Wu criterion for bearing analysis.

The models developed for the net tension and shearout failure did not deal with changes in material anisotropy and the resultant effects on the strength. If the anisotropy (orthotropy) is defined by the ratio of inplane longitudinal modulus to transverse modulus, the effects on the inplane stress distributions can be studied as a function of anisotropy ratio. Some preliminary work indicates that the primary effect of anisotropy is to change the shape of the stress distributions. The location of the point of maximum stress remains the same however. By formulating approximate stress functions for the different anisotropy conditions the models can be

incorporated into the failure criteria without changing the accuracy of the strength predictions. More research both analytical and experimental needs to be done in order to fully understand the effects of anisotropy.

CONCLUSIONS

The failure behavior of composite bolted joints has been investigated for the three primary failure modes, bearing, shearout and net tension. Strength analyses were developed for each mode and their accuracy determined by comparison with empirical data.

The analysis of composite bolted joint strength is dependent upon determination of the state of stress in the joint and the application of an appropriate failure criterion. A two-dimensional, plane stress, finite-element model was found to accurately predict stresses along the net tension and shearout planes as verified by comparison with experimental results. The plane stress assumption appears to be invalid for analysis of stresses near fastener hole in the bearing region of the joint. The predicted stresses appear to be approximately one half the magnitude measured by strain gages. Since the interlaminar stresses could significantly affect the strength of the laminate in this region it is suggested that a three-dimensional analysis be developed.

Parametric studies performed to evaluate the effect of joint geometry on the state of stress around

the joint revealed the existence of relatively simple relationships between maximum stress and geometry. This allowed development of functional form approximating the stress profiles for each failure mode. This development of analytical approximation of the stresses as a function of joint is important in the reduction of the empirical data base needed in composite joint design.

Semi-empirically based strength analyses were developed for each failure mode by application of the failure criteria and the stress analysis. After comparison with experimental data it was concluded that failure models using the "point stress" criterion for net tension and shearout failure modes accurately predict bolted joint strengths for the laminate configuration and geometries investigated. The questionable accuracy of the plane stress analysis for the bearing made prohibited any conclusions about the applicability of the Tsai-Wu failure criterion.

The development of an approximate closed form strength analysis based on the "point stress" criterion and incorporated geometric effects results in a potential reduction in the empirical data base required for bolted joint design. The expansion of this concept to include the bearing mode and effects of material anisotropy and environment could lead to the development of a comprehensive bolted joint design procedure.

REFERENCES

1. Waszczak, J. P. and Cruse, T. A., "Failure Mode and Strength Predictions of Anisotropic Bolt Bearing Specimens," J. of Composite Materials, Vol. 5, July 1971, p. 421.

2. Waszczak, J. P. and Cruse, T. A., "A Synthesis Procedure for Mechanically Fastened Joints in Advanced Composite Materials," AIAA/ASME/SAE 14th Structures, Structural Dynamics, and Materials Conference, March 1973.

3. Soni, R. Som, "Failure Analysis of Composite Laminates with a Fastener Hole," Materials Laboratory, Air Force Wright Aeronautical Laboratories, Technical Report AFWAL-TR-80-4010, March 1980.

4. Harris, H. G. and Ojalvo, I. U., "Simplified Three-Dimensional Analysis of Mechanically Fastened Joints," Proceedings of the Army Symposium on Solid Mechanics, AMMRC MS74-8, September 1974.

5. Jong, Theo de, "Stresses Around Pin-Loaded Holes in Elastically Orthotropic or Isotropic Plates," J. Composite Materials, Vol. 11, July 1977, p. 313.

6. Oplinger, D. W. and Gandhi, R. R., "Stresses in Mechanically Fastened Orthotropic Laminates," Proceedings of the Second Conference on Fibrous Composites in Flight Vehicle Design, May 21-24, 1974, Dayton, Ohio.

7. Eisenmann, J. R., "Bolted Joint Static Strength Model for Composite Materials," NASA-TM-X-3377, 1976.

8. Ramkumar, R. L., "Bolted Joint Design," Proc. of ASTM Symposium on Test Methods and Design Allowables for Fibrous Composites, Dearborn, Michigan, October 3-4, 1979.

9. Hart-Smith, L. J., "Bolted Joints in Graphite-Epoxy Composites," Douglas Aircraft Company, NASA Contract Report NASA CR-144899, June 1976.

10. Advanced Composites Design Guide, Vol. I, Design, Third Edition, Contract F33615-74-C-5075, North American Rockwell/Los Angeles Division, January 1973.

11. Van Siclen, R. C., "Evaluation of Bolted Joints in Graphite-Epoxy," Proceedings of the Army Symposium on Solid Mechanics, AMMRC MS74-8, September 1974.

12. Collins, T. A., "The Strength of Bolted Joints in Multi-Directional CFRP Laminates," Composites, Vol. 8, January 1977.

13. Hyer, M. W. and Lightfoot, M. C., "Ultimate Strength of High-Load-Capacity Composite Bolted Joints," Composite Materials: Testing and Design (Fifth Conference), ASTM STP 674, S. W. Tsai (Ed.), American Society for Testing and Materials, 1979, pp. 118-136.

14. Quinn, W. J. and Matthews, F. L., "The Effect of Stacking Sequence on the Pin-Bearing Strength in Glass Fibre Reinforced Plastic," J. Composite Materials, Vol. 11, April 1977, p. 139.

15. Wilson, D. W. and Pipes, R. B., "Behavior of Composite Bolted Joints at Elevated Temperature," University of Delaware Center for Composite Materials, NASA Contract Report 159137, September 1979.

16. Wilson, D. W., Pipes, R. B., Webster, J. W. and Riegner, D. L., "Mechanical Characterization of PMR-15 Graphite/Polyimide Bolted Joints," Proceedings of ASTM Symposium on Test Methods and Design Allowables for Fibrous Composites, Dearborn, Michigan, October 3-4, 1979.

17. Kim, R. Y. and Whitney, J. M., "Effect of Temperature and Moisture on Pin Bearing Strength of Composite Laminates," J. Composite Materials, Vol. 10, April 1976, P. 149.

18. Wilkins, D. J., "Environmental Sensitivity Tests of Graphite-Epoxy Bolt Bearing Properties," Composite Materials: Testing and Design (Fourth Conference), ASTM STP 617, American Society for Testing and Materials, 1977, pp. 497-513.

19. "Standard Test Method for Tensile Properties of Oriented Fiber Composites," ASTM D-3039-76, ASTM Standards, Part 35.

20. Hofer, Kenneth E., Rao, P. N. and Humphreys, V. E., "Development of Engineering Data on the Mechanical and Physical Properties of Advanced Composite Materials," AFML TR-72-205, Part I, IIT Research Institute, 1972.

21. Garcia, R., Weisshaar, T. A. and McWithey, R. R., "An Experimental and Analytical Investigation of the Rail Shear-Test Method as Applied to Composite Materials," Experimental Mechanics, Volume 20, No. 8, August 1980.

22. Nuismer, R. J. and Whitney, J. M., "Uniaxial Failure of Composite Laminates Containing Stress Concentrations," Fracture Mechanics of Composites, ASTM STP 593, 1975.

23. Pipes, R. B., Wetherhold, R. C. and Gillespie, J. W., J. Comp. Mater., 12, 148, 1979.

24. Pipes, R. B., Gillespie, J. W. and Wetherhold, R. C., Polymer Eng. and Sci., Vol. 15, No. 16, 1979.

25. Wu, E. M., "Optimal Experimental Measurements of Anisotropic Failure Tensors," J. Comp. Mater., Vol. 6, October 1972.

26. Stockdale, J. H. and Matthews, F. L., "The Effect of Clamping Pressure on Bolt Bearing Loads in Glass Fibre Reinforced Plastics," Composites, 1976.

APPENDIX A

Table 2a.

Bolt Bearing Strength Data
(English Units)

Specimen Number	Hole Diameter D (in.)	Width W (in.)	Thickness t (in.)	Edge Distance e (in.)	Maximum Load (lbs.)	Far-Field Failure Stress σ_o (ksi)
7-1B-2R	.131	.251	.120	.452	1169	38.7
7-1B-5L	.131	.252	.118	.452	1279	42.9
7-1B-6L	.132	.251	.117	.453	1125	38.2
6-2A-4L	.260	.503	.118	.928	838	36.3
6-2A-4R	.260	.504	.118	.925	2272	38.1
6-2A-8R	.259	.502	.119	.932	2250	37.6
6-2A-1R	.386	.746	.117	1.367	3573	40.8
6-2A-3L	.386	.752	.119	1.378	3485	38.8
6-2A-3R	.386	.752	.119	1.370	3573	39.8

Table 2b.

Bolt Bearing Strength Data
(S.I. Units)

Specimen Number	Hole Diameter D (mm)	Width W (mm)	Thickness t (mm)	Edge Distance e (mm)	Maximum Load ($Nt \times 10^3$)	Far-Field Failure Stress σ_o (MPa)
7-1B-2R	3.33	6.38	3.05	11.48	5.20	266.8
7-1B-5L	3.33	6.40	3.00	11.48	5.69	295.5
7-1B-6L	3.35	6.38	2.97	11.51	5.00	263.4
6-2A-4L	6.60	12.78	3.00	23.57	3.73	250.3
6-2A-4R	6.60	12.75	3.00	23.50	10.10	262.7
6-2A-8R	6.58	12.75	3.02	23.67	10.00	259.3
6-2A-1R	9.80	18.95	2.97	34.72	15.89	281.3
6-2A-3L	9.80	19.10	3.02	35.00	15.49	267.5
6-2A-3R	9.80	19.10	3.02	34.80	15.89	274.4

Table 3a.

Pin Bearing Strength Data
(English Units)

Specimen Number	Hole Diameter D (in.)	Width W (in.)	Thickness t (in.)	Edge Distance e (in.)	Maximum Load (lbs.)	Far-Field Failure Stress σ_o (ksi)
7-1B-5R	.131	.252	.118	.454	1324	44.4
7-1B-7L	.131	.252	.115	.450	1213	41.8
7-1B-7R	.132	.252	.116	.452	1279	43.7
6-2A-8L	.260	.503	.119	.929	2425	40.4
7-1B-4L	.259	.501	.118	.926	2470	41.7
7-1B-4R	.260	.501	.118	.930	2294	38.7
6-1B-1R	.385	.750	.118	1.378	3441	38.8
6-2A-1L	.385	.747	.118	1.376	3441	38.9
6-1B-1L	.384	.750	.118	1.377	3397	38.3

Table 3b.

Pin Bearing Strength Data
(S.I. Units)

Specimen Number	Hole Diameter D (mm)	Width W (mm)	Thickness t (mm)	Edge Distance e (mm)	Maximum Load ($Nt \times 10^3$)	Far-Field Failure Stress σ_o (MPa)
7-1B-5R	3.33	6.40	3.00	11.53	5.88	306.14
7-1B-7L	3.33	6.40	2.92	11.43	5.39	288.2
7-1B-7R	3.35	6.40	3.95	11.48	5.69	301.3
6-2A-8L	6.60	12.78	3.02	23.60	10.79	278.6
7-1B-4L	6.58	12.73	3.00	23.52	10.98	287.5
7-1B-4R	6.60	12.73	3.00	23.62	10.20	266.8
6-1B-1R	9.78	19.05	3.00	35.00	15.30	267.5
6-2A-1L	9.78	18.97	3.00	34.95	15.30	268.2
[illegible]	9.75	19.05	3.00	34.98	15.10	264.08

Table 4a.

Shearout Strength of Bolted Joints
(English Units)

Specimen Number	Hole Diameter D (in.)	Width W (in.)	Thickness t (in.)	Edge Distance e (in.)	Maximum Load (lbs.)	Far-Field Failure Stress σ_o (ksi)
8-2A-1R	0.125	0.750	0.116	.250	1345	15.5
6-2B-4R	0.125	0.750	0.120	.249	1324	14.7
8-1B-4L	0.125	0.751	0.118	.248	1324	14.9
8-2A-2R	0.250	1.497	0.119	.504	3044	17.1
6-2B-3R	0.250	1.496	0.120	.508	3066	17.4
8-2A-2L	0.250	1.497	0.118	.506	2823	16.0
7-1A-1L	0.375	2.252	0.119	.748	4522	16.9
7-1A-1R	0.375	2.252	0.118	.746	4634	17.3
7-1A-3L	0.375	2.251	0.120	.756	4412	16.3

Table 4b.

Shearout Strength of Bolted Joints
(S.I. Units)

Specimen Number	Hole Diameter D (mm)	Width W (mm)	Thickness t (mm)	Edge Distance e (mm)	Maximum Load ($Nt \times 10^3$)	Far-Field Failure Stress σ_o (MPa)
8-2A-1R	3.38	19.05	2.95	6.35	3.98	106.9
6-2B-4R	3.34	19.05	3.05	6.32	5.89	101.4
8-1B-4L	3.33	19.08	3.00	6.30	5.89	102.7
8-2A-2R	6.60	38.02	3.02	12.80	13.53	117.9
6-2B-3R	6.61	38.00	3.05	12.90	13.63	117.9
8-2A-2L	6.58	38.02	3.00	12.85	12.55	110.3
7-1A-1L	9.78	57.20	3.02	19.00	20.10	116.5
7-1A-1R	9.78	57.20	3.00	18.95	20.60	119.3
7-1A-3L	9.80	57.18	3.05	19.20	19.61	112.4

Table 5a.

Shearout Strength of Pin Loaded Joints
(English Units)

Specimen Number	Hole Diameter D (in.)	Width W (in.)	Thickness t (in.)	Edge Distance e (in.)	Maximum Load (lbs.)	Far-Field Failure Stress σ_o (ksi)
8-1A-1R	0.131	0.750	0.117	0.250	1213	28.3
6-2A-2L	0.128	0.751	0.119	0.246	1103	25.3
8-2A-1L	0.131	0.751	0.114	0.250	1058	25.4
6-2B-3L	0.258	1.496	0.120	0.506	2184	24.1
6-1A-2L	0.261	1.502	0.121	0.504	1786	20.1
6-1A-2R	0.259	1.502	0.117	0.502	2382	27.0
7-1A-2R	0.385	2.247	0.117	0.746	3662	27.7
7-1A-2L	0.385	2.247	0.119	0.746	3750	28.3
7-1A-3R	0.384	2.251	0.120	0.750	3640	27.3

Table 5b.

Shearout Strength of Pin Loaded Joints
(S.I. Units)

Specimen Number	Hole Diameter D (mm)	Width W (mm)	Thickness t (mm)	Edge Distance e (mm)	Maximum Load ($Nt \times 10^3$)	Far-Field Failure Stress σ_o (MPa)
8-1A-1R	3.33	19.05	2.97	6.35	5.39	195.1
6-2A-2L	3.25	19.07	3.02	6.25	4.90	174.4
8-2A-1L	3.33	19.07	2.90	6.35	4.70	175.1
6-2B-3L	6.55	38.00	3.05	12.85	9.71	166.2
6-1A-2L	6.63	38.15	2.97	12.80	7.93	138.6
6-1A-2R	6.53	38.15	2.97	12.75	10.59	186.2
7-1A-2R	9.78	57.07	2.97	18.95	16.28	191.0
7-1A-2L	9.78	57.07	3.02	18.95	16.67	195.1
7-1A-3R	9.76	63.75	3.05	19.05	16.18	188.2

Table 6a.

Net Tension Strength of Bolted Joints
(English Units)

Specimen Number	Hole Diameter D (in.)	Width W (in.)	Thickness t (in.)	Edge Distance e (in.)	Maximum Load (lbs.)	Far-Field Failure Stress σ_o (ksi)
6-2A-2R	0.131	0.750	0.118	0.504	1301	14.7
6-2B-4L	0.133	0.750	0.120	0.502	1191	13.2
8-1B-4R	0.131	0.752	0.119	0.498	1213	13.6
7-1B-1L	0.261	1.504	0.121	1.006	2536	13.9
8-1B-3L	0.257	1.496	0.119	1.006	2647	14.8
7-1B-2L	0.258	1.499	0.118	1.009	2338	13.2
8-2A-3L	0.388	2.250	1.120	1.362	3397	12.6
6-2B-2L	0.388	2.249	0.119	1.366	3750	14.0
8-2A-3R	0.389	2.250	0.120	1.366	3861	14.3

Table 6b.

Net Tension Strength of Bolted Joints
(S.I. Units)

Specimen Number	Hole Diameter D (mm)	Width W (mm)	Thickness t (mm)	Edge Distance e (mm)	Maximum Load ($Nt \times 10^3$)	Far-Field Failure Stress σ_o (MPa)
6-2A-2R	3.33	19.05	3.00	12.80	5.78	101.4
6-2B-4L	3.38	19.05	3.05	12.75	5.29	91.0
8-1B-4R	3.33	19.10	3.02	12.65	5.39	91.0
7-1B-1L	6.63	38.20	3.07	25.55	11.27	95.8
8-1B-3L	6.53	38.00	3.02	25.55	11.77	102.1
7-1B-2L	6.55	38.07	3.00	25.63	10.39	91.0
8-2A-3L	9.86	57.15	3.05	34.59	15.10	86.9
6-2B-2L	9.86	57.12	3.02	34.70	16.67	96.5
8-2A-3R	9.88	57.15	3.05	34.70	17.16	98.6

Table 7a.

Net Tension Strength of Pin Loaded Joints
(English Units)

Specimen Number	Hole Diameter D (in.)	Width W (in.)	Thickness t (in.)	Edge Distance e (in.)	Maximum Load (lbs.)	Far-Field Failure Stress σ_o (ksi)
7-1B-3R	0.257	1.499	0.110	1.006	3485	19.5
8-1A-2R	0.259	1.497	0.120	1.004	3485	19.4
7-1B-1R	0.259	1.504	0.119	1.004	3618	20.2
6-2B-2R	0.388	2.249	0.120	1.366	5427	20.1
8-1B-2R	0.388	2.250	0.120	1.360	5074	18.8
8-1B-2L	0.388	2.250	0.120	1.365	5294	19.64

Table 7b.

Net Tension Strength of Pin Loaded Joints
(S.I. Units)

Specimen Number	Hole Diameter D (mm)	Width W (mm)	Thickness t (mm)	Edge Distance e (mm)	Maximum Load ($Nt \times 10^3$)	Far-Field Failure Stress σ_o (MPa)
7-1B-3R	6.53	38.07	3.02	25.55	15.49	134.5
8-1A-2R	6.58	38.02	3.05	25.55	15.49	133.8
7-1B-1R	6.58	38.20	3.02	25.55	16.08	139.3
6-2B-2R	9.86	57.12	3.05	33.70	24.12	138.6
8-1B-2R	9.86	57.15	3.05	34.54	22.55	129.6
8-1B-2L	9.86	57.25	3.05	34.67	23.53	135.1